Unbiased Gradient Low-Rank Projection

Rui Pan♠*,   **Yang Luo**♣*   **Yuxing Liu**♠*   **Yang You**♣   **Tong Zhang**♠

♠University of Illinois Urbana-Champaign
♣National University of Singapore
{ruip4, yuxing6, tozhang}@illinois.edu
{yangluo, youy}@comp.nus.edu.sg

Abstract

Memory-efficient optimization is critical for training increasingly large language models (LLMs). A popular strategy involves gradient low-rank projection, storing only the projected optimizer states, with GaLore being a representative example. However, a significant drawback of many such methods is their lack of convergence guarantees, as various low-rank projection approaches introduce inherent biases relative to the original optimization algorithms, which contribute to performance gaps compared to full-parameter training. Aiming to tackle this problem, this paper investigates the layerwise sampling technique for debiasing low-rank projection mechanisms. In particular, an instantiation of the paradigm gives rise to a novel and unbiased low-rank optimization method built upon GaLore's mechanism and the Muon algorithm, named GaLore Unbiased with Muon (GUM). We theoretically prove our method matches the convergence guarantees of the base Muon algorithm while preserving the memory efficiency of low-rank techniques. Empirical experiments on LLM fine-tuning and pretraining also demonstrate non-trivial improvements over GaLore and even better performance than full-parameter training. Further investigation shows that the improvement of this technique comes from a more uniform distribution of knowledge inside layers, leading to more efficient utilization of the model parameter space and better memorization.

1 Introduction

Large language models (LLMs) have demonstrated impressive performance across a diverse range of tasks, including conversation [Ouyang et al., 2022, Grattafiori et al., 2024a], mathematical reasoning [Guo et al., 2025], and agentic applications [Qin et al., 2025]. The advancement of these powerful LLMs demands substantial GPU memory due to the large size of the underlying models. For example, training a 70B model with full parameters requires approximately 1.2 terabytes of GPU memory, which exceeds the capacity of even $8 \times$H100 GPUs.

To address this issue, memory-efficient training techniques such as GaLore [Zhao et al., 2024] have been introduced. GaLore projects gradients into a low-rank space, reducing the memory footprint of optimizer states during training. Specifically, it employs the top-r components from Singular Value Decomposition (SVD) to define a compact low-rank space, into
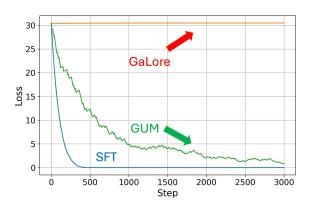

Figure 1: A counterexample of GaLore in linear regression with Muon optimizer [Jordan et al., 2024], where its debiased version GUM converges while GaLore fails to converge.

which the gradients are projected as $R_t \leftarrow P_t^\top G_t$. The optimization step is then performed in this low-rank space, enabling memory savings for the optimizer states. For example, the first and second moments in Adam [Kingma and Ba, 2014] are updated using $\tilde{M}_t \leftarrow \beta_1 \tilde{M}_{t-1} + (1 - \beta_1)R_t$ and $\tilde{V}_t \leftarrow \beta_2 \tilde{V}_{t-1} + (1 - \beta_2)R_t$, where the

---

*Equal Contribution.

Algorithm 1 Low-rank projection based gradient descent algorithms
___

1: **Input:** Initial weight $W_0 \in \mathbb{R}^{m \times n}$ (suppose $m \leq n$), number of iterations K, learning rate η, projection rank r.
2: **for** $t = 0$ **to** $K - 1$ **do**
3:      $G_t = G(W_t)$ $\triangleright$ Obtain the gradient at W_t
4:      $P_t \leftarrow$ `get_projector()` $\triangleright$ Obtain the projector $P_t \in \mathbb{R}^{m \times r}$
5:      $\tilde{G}_t = P_t^\top G_t$ $\triangleright$ Obtain projection of the gradient in the low-rank space
6:      $S_t \leftarrow$ `optimizer.update_state(`$\tilde{G}_t$`)` $\triangleright$ Run the base algorithm with $\tilde{G}_t$
7:      $W_{t+1} = W_t - \eta P_t S_t$ $\triangleright$ Project the update back and update the weights
8: **end for**
___

low-rank projected gradient R_t replaces the original gradient G_t. After the optimization step, the parameter update is projected back to the original space.

Nevertheless, most low-rank optimization methods introduce biased gradient estimations during training [Muhamed et al., 2024, Zhang et al., 2024a, He et al., 2024, Huang et al., 2025], which can lead to suboptimal convergence behavior and measurable performance gaps compared to standard full-parameter training. These biases arise because low-rank projections, while computationally and memory efficient, do not fully preserve the direction and magnitude of the true gradient, especially in high-dimensional parameter spaces. As a result, the optimization trajectory diverges from that of full-precision training, potentially causing slower convergence, reduced final model quality, or instability in certain regimes [Zhao et al., 2024, Ding et al., 2022, Zhang et al., 2024a, Huang et al., 2025]. This limitation is particularly critical when pre-training large language models (LLMs), where even small discrepancies in gradient estimation can propagate and amplify across many layers and iterations.

To address this fundamental issue, we investigate the general debiasing technique using layerwise sampling [Pan et al., 2024], which preserves the memory efficiency of training methods via randomly freezing most of the layers. Specifically, the unique strength of layerwise sampling over the typical low-rank projected algorithms of GaLore is analyzed both theoretically and empirically. The introduction of the debiasing technique into GaLore gives rise to a new algorithm called **Galore Unbiased with Muon (GUM)**, which demonstrates much better convergence guarantees and practical performance in LLM training tasks. We summarize our major contributions as follows:

- We investigate the layerwise-sampling debiasing technique and propose a novel algorithm called **G**aLore **U**nbiased with **M**uon (**GUM**), which unifies the strengths of GaLore and Muon. GUM achieves the same theoretical convergence guarantees as Muon while retaining the memory efficiency of GaLore, enabling scalable and effective training of large models.

- Empirical experiments in LLM training demonstrate that GUM consistently outperforms GaLore in instruction-following, mathematical reasoning, and commonsense reasoning tasks under the same memory budget. Surprisingly, in LLM pre-training experiments, GUM even outperforms full-parameter trained AdamW by a non-trivial overall accuracy margin of 0.3%-1.1%, while obtaining on-par or better performance than AdamW in 6 out of 7 tasks.

- We analyze the underlying reasoning of GUM's empirical improvements, discovering that its high-rank update nature leads to a larger overall stable rank and more evenly distributed singular values in model weights, which further induce a more long-tailed activation pattern in trained models. This implies the performance gain is brought by more efficient utilization of the model parameter space, in other words, better memorization.

2 Related Work

Parameter-Efficient Algorithms in Practice. Parameter-Efficient Fine-Tuning (PEFT) methods are widely adopted for training large-scale LLMs in practice. A typical approach is LoRA [Hu et al., 2022], which freezes the original model and attaches a small trainable low-rank adapter, thereby reducing memory consumption and improving training efficiency. However, LoRA has been reported to exhibit a non-trivial performance gap compared to full-parameter training [Ding et al., 2022, Lialin et al., 2023], due to its altered parameter space. These changes in parameter space also introduce theoretical challenges in analyzing LoRA's convergence

properties with respect to the original parameter space. To address the aforementioned deficiencies and extend LoRA to larger-scale training settings, GaLore [Zhao et al., 2024] proposes a different approach, which projects the gradients—rather than the parameters—into low-rank spaces. In doing so, the error between the full gradients and the approximated gradients becomes numerically quantifiable, as they now operate within the same parameter space.

Following GaLore, a number of low-rank projection-based algorithms have emerged, where the key component follows a similar paradigm to Algorithm 1, but with different projection matrices P. GaLore utilizes the top-r entries $U[:,:r]$ from SVD, which is computationally expensive. To address this issue, GRASS [Muhamed et al., 2024] derives a sparse projection matrix P based solely on the row norms of the gradients. Specifically, each projection entry is sampled from a multimodal distribution proportional to the row norms. GRASS has been reported to achieve performance comparable to GaLore with lower computational cost, though no theoretical guarantees have been provided regarding its convergence. LoGE [Zhang et al., 2024a] obtains the low-rank projection P by decomposing the original weight matrix $W = BC$, thereby implicitly allowing the backward gradient to be low-rank. However, it is difficult to guarantee theoretical convergence due to the empirical nature of the low-rank decomposition. GradNormLoRP [Huang et al., 2025] combines ideas from LoRA and GaLore, resulting in a two-level projection P that further enhances memory efficiency and reduces training cost. A variety of salience-aware sparse projections are also employed in [Guo et al., 2020, Sung et al., 2021, Ansell et al., 2021, Das et al., 2023, Liu et al., 2024a], each using different saliency metrics.

Despite the strong empirical performance across various practical settings, most of the aforementioned methods lack guarantees regarding their theoretical convergence rates, which can be attributed to the biasedness of the projected gradients. To bridge this gap, we investigate the debiasing technique of layerwise-sampling that compensates for the errors introduced by low-rank projected updates, aiming to improve their theoretical convergence guarantees while maintaining practical memory efficiency.

Unbiased Optimization Methods. The research on unbiased methods is an important part of the optimization field, especially for distributed and memory-efficient optimization. This includes methods of unbiased quantization [Alistarh et al., 2017, Suresh et al., 2017, Wang et al., 2022] and unbiased sparsification [Wangni et al., 2018, Stich et al., 2018, Wang et al., 2018]. The unbiased property of these methods enables low communication/memory burden while maintaining guaranteed convergence. For the recently popular low-rank projection-based methods, Fira [Chen et al., 2024] provides an attempt to involve full-rank information by adding a scaled gradient projection to the update, but without a rigorous theoretical justification of the approach. GoLore [He et al., 2024] is probably the closest to building an unbiased algorithm. However, they employ a totally random projection matrix for the algorithm to enable the convergence guarantee, which may fail to capture the loss landscape properties and lead to slow convergence.

Muon Optimizer. Muon [Jordan et al., 2024] is a novel optimizer proposed recently, which is gaining rapidly increasing attention because of its great potential in training large foundation models [Liu et al., 2025a, Kimi, 2025], empirically outperforming AdamW on specific large-scale tasks. On the theoretical side, An et al. [2025], Li and Hong [2025] proves its non-convex deterministic and stochastic convergence, respectively, showing a strong theoretical guarantee for the optimizer.

3 Algorithm

3.1 GaLore Unbiased with Muon

As previously shown in Algorithm 1, the core of low-rank gradient methods is to only store the low-rank projected optimizer states, i.e., related to $\tilde{G}_t \in \mathbb{R}^{m \times r}$, which is then projected back to the weight space by multiplying P_t to update the weight W_t. The update conceptually shares similarities with running the base optimizer using low-rank projected gradients $P_t P_t^\top G_t$ instead of G_t.

This inspires the key idea of *debiasing*, that is, to compensate for biased errors introduced by the low-rank projection $P_t P_t^\top G_t$. To implement this while retaining memory efficiency, we refer to the main idea of LISA [Pan et al., 2024], which allows some of the blocks to be sampled uniformly with probability q in each period. This compensated full-rank updates use $G_t - P_t P_t^\top G_t$, while other blocks still do the original low-rank update. By carefully balancing the scaling constants for the two different updates, the biased low-rank term can be canceled out in expectation, resulting in an unbiased estimation of gradients across iterations. Due to page limit, we present this general unbiased algorithm paradigm in Algorithm 3 in Appendix A.

For a practical instance of this paradigm, we consider applying GaLore as the low-rank projection method and Muon as the base algorithm, which gives birth to our proposed optimization algorithm, called **G**aLore **U**nbiased

Algorithm 2 GaLore Unbiased with **M**uon (**GUM**)

1: **Input:** $\{W_{0,\ell} \in \mathbb{R}^{m_\ell \times n_\ell}\}$ with each ℓ corresponding to the ℓ-th block of parameters, number of blocks N_L, sampling period K, rank r for each layer, full-rank update layer number γ
2: **for** $t = 0$ **to** $T/K - 1$ **do**
3:     **for** $\ell = 1$ **to** N_L **do**
4:         Initialize $R_{t,0,\ell} = 0$ ▷ Restart the momentum to clear memory
5:         $G_{t,0,\ell} = G(W_{t,\ell})$ ▷ Obtain the gradient of the ℓ-th layer at W_t
6:         $U_{t,\ell}, S_{t,\ell}, V_{t,\ell} = \mathrm{SVD}(G_{t,0,\ell})$ ▷ Compute SVD of gradient obtained at W_{tK}
7:         $P_{t,\ell} = U_{t,\ell}[:,:r]$ ▷ Obtain GaLore projector $P_{t,\ell} \in \mathbb{R}^{m \times r}$ (suppose $m_\ell \leq n_\ell$)
8:     **end for**
9:     Each block ℓ is sampled to do full-rank updates with probability $q_{t,\ell} \equiv q = \frac{\gamma}{N_L}$
10:     **for** $k = 0$ **to** $K - 1$ **do**
11:         Run (1) for all blocks sampled to compute low-rank update
12:         Run (2) for all blocks sampled to compute full-rank update
13:     **end for**
14: **end for**

---

with **M**uon (**GUM**), as presented in Algorithm 2.

In one training process, the algorithm contains separated periods just like the vanilla GaLore and LISA. During each period t, each block of parameters is sampled to do full-rank updates with probability $q_{t,\ell}$. In each iteration k in the period, we first compute the projection matrix $P_{t,k,\ell}$ and sample the layers to do full-rank updates in this period.

If block ℓ is sampled to do the low-rank update, we apply the following update adapted from Muon with $G_{t,k,\ell} = G(W_{tK+k,\ell})$ as the gradient of block ℓ at iteration k in period t:

$$
\begin{aligned}
R_{t,k,\ell} =& \beta R_{t,k-1,\ell} + \frac{1}{1 - q_{t,\ell}} P_{t,\ell}^\top G_{t,k,\ell} \\
W_{Kt+k+1,\ell} =& W_{Kt+k,\ell} + \eta_{t,k} P_{t,\ell} \mathrm{NewtonSchulz}(R_{t,k,\ell})
\end{aligned}
\tag{1}
$$

Note that if we set $q_{t,\ell} = 0$, (1) is exactly GaLore with Muon as the base optimizer, which we will refer to as GaLore-Muon. In terms of memory consumption, we can see that the optimizer states requiring storage are the projection matrix $P_{t,\ell} \in \mathbb{R}^{m_\ell \times r}$ and $R_{t,k,\ell} \in \mathbb{R}^{r \times n_\ell}$. Otherwise, the block is sampled to compute high-rank updates, and the compensated projection update is applied.

$$
\begin{aligned}
R_{t,k,\ell} =& \beta R_{t,k-1,\ell} + \frac{1}{q_{t,\ell}} \left(G_{t,k,\ell} - P_{t,\ell} P_{t,\ell}^\top G_{t,k,\ell} \right) \\
W_{tK+k+1,\ell} =& W_{tK+k,\ell} + \eta_{t,k} \mathrm{NewtonSchulz}(R_{t,k,\ell})
\end{aligned}
\tag{2}
$$

In this case, $P_{t,\ell} \in \mathbb{R}^{m_\ell \times r}$ and $R_{t,k,\ell} \in \mathbb{R}^{m_\ell \times n_\ell}$ are required to be stored.

Summarizing both cases, the overall memory consumption comparison with the vanilla GaLore-Muon algorithm is obtained, as shown in Table 3. The memory consumption of GUM is higher than that of GaLore when using the same projection rank r, due to the use of probabilistic full-rank updates. However, as demonstrated in Section 5, by employing a smaller projection rank r' as a trade-off, the benefits of this additional memory consumption are sufficient to recover the performance loss and even achieve a smaller overall memory footprint.

We can show that this update is unbiased compared to the original Muon update.

Lemma 1 (GUM is unbiased). *A single iteration of Algorithm 2 for $W \in \mathbb{R}^{m \times n}$ is equivalent to*

$$
\begin{aligned}
\tilde{M}^+ =& \beta \tilde{M} + \tilde{G} \\
W^+ =& W - \eta \mathrm{NewtonSchulz}(\tilde{M}^+)
\end{aligned}
$$

with $\mathbb{E}[\tilde{G}] = G \in \mathbb{R}^{m \times n}$, where G denotes the gradient obtained at W.

This unbiased technique is crucial for the convergence of the algorithm. As we will see in the next subsection, GUM can recover similar convergence properties as the original Muon algorithm, regardless of the employed projection matrix. This demonstrates substantial theoretical advantages over the original biased GaLore-Muon algorithm.

4 Convergence Analysis of GUM

In this section, we present the convergence analysis of GUM. We consider the following assumptions for the minimization problem $\min_{W \in \mathbb{R}^{m \times n}} f(W)$ with $m \leq n$.

Assumption 1 (Lower bounded). *There exists $f^* > -\infty$ such that $f(W) \geq f^*$ for all $W \in \mathbb{R}^{m \times n}$.*

Assumption 2 (Smoothness). *f is L_{op}-smooth with respect to the spectral norm $\|\cdot\|_{\mathrm{op}}$, i.e.,*

$$\|\nabla f(W_1) - \nabla f(W_2)\|_* \leq L_{\mathrm{op}} \|W_1 - W_2\|_{\mathrm{op}},$$

for all $W_1, W_2 \in \mathbb{R}^{m \times n}$. $\|\cdot\|_{\mathrm{op}}$ and $\|\cdot\|_*$ denotes the spectral norm and trace norm respectively.

Assumption 3 (Gradient noise). *We assume the stochastic gradient $G(W)$ obtained at W is unbiased and there exists a matrix $V \in \mathbb{R}^{m \times n}$ such that*

$$\mathbb{E}[N(W)] = 0 \quad \text{and} \quad \mathbb{E}\left[N(W)N(W)^\top\right] \preceq VV^\top,$$

where $N(W) \triangleq G(W) - \nabla f(W)$ and $A \preceq B$ denotes that $B - A$ is positive semidefinite.

Assumption 1 is standard in non-convex analysis. Based on the equivalence between norms, Assumption 2 implies nothing more than the standard smoothness assumption on Frobenius norm, but is more suitable in analyzing GUM or Muon [Jordan et al., 2024]. Assumption 3 can also imply the standard bounded variance assumption by $\mathbb{E}[\|N(W)\|_{\mathrm{F}}^2] \leq \|V\|_{\mathrm{F}}^2$. The style of these assumptions can be found in previous work on analyzing adaptive methods and Sign-based methods [Bernstein et al., 2018, Crawshaw et al., 2022, Liu et al., 2024b, An et al., 2025], where the assumptions are employed for more fine-grained analysis and analyzing the potential benefits of these optimizers.

Assumption 4 (Exact Newton Schulz). *We consider the case where the Newton-Schulz iteration computes the exact solution, i.e., `NewtonSchulz`$(X) = UV^\top$ with $X = U\Sigma V^\top$ as the SVD of X.*

Assumption 4 is needed for analyzing Muon. As noted in Jordan et al. [2024], Liu et al. [2025a], though the Newton-Schulz iteration adopted in Muon does not compute the exact $UV^\top$ matrix, it turns out that this error has little influence on the training curve. Then, based on the assumptions, we can obtain the convergence guarantee for GUM.

Theorem 1 (Non-convex Convergence). *Under Assumption 1-4, after running a total of T iterations for Algorithm 2 with parameters set as* (12)*, it holds that*

$$\min_{0 \leq s \leq T-1} \mathbb{E}\left[\|\nabla f(W_s)\|\right] \leq \mathcal{O}\left(\frac{1}{\alpha}\sqrt{\frac{L_{\mathrm{op}}\Delta}{T}} + \left(\frac{L_{\mathrm{op}}\Delta \|V\|_*^2}{\alpha^5 T}\right)^{\frac{1}{4}} + \frac{\|V\|_*}{\sqrt{\alpha^3 T}}\right),$$

where $\Delta \triangleq f(W_0) - f^*$ and $\alpha \triangleq \min\{q, 1-q\}$.

The proof can be found in Appendix B. The convergence theorem for GUM leads to several important observations. Firstly, when we set q to be an absolute constant, the convergence of GUM matches exactly the convergence rate of Muon. In the deterministic case, it matches the convergence result of Muon proven in An et al. [2025]. When the noise V is the dominant term, it also matches the $\mathcal{O}(T^{-1/4})$ rate proven in Li and Hong [2025]. Moreover, since we use more fine-grained and appropriate assumptions to analyze GUM, Theorem 1 shows an even better dimensional dependence than Li and Hong [2025]. This consistency shows the power of the unbiased design, maintaining the memory reduction of gradient low-rank methods without sacrificing the convergence guarantee.

As noted by He et al. [2024], GaLore using SGD with momentum (SGDM) as the base algorithm converges in the deterministic non-convex setting, but can possibly diverge when the gradient noise is large. We also empirically examine an extreme counterexample where GaLore-Muon doesn't converge at all in Section 5. Clearly, GUM fixes this problem. GoLore [He et al., 2024] is also designed to correct the convergence of GaLore. However, though GoLore shows a good convergence guarantee when the base algorithm is SGDM, it employs a thoroughly random projection matrix to do low-rank updates, failing to capture the potential gradient low-rank properties as the GaLore projection matrix does. This can lead to a much slower convergence speed when applied to real training tasks.

5 Experimental Results

5.1 Synthetic Settings

To better illustrate how GaLore may fail due to the low-rank projection, we consider the following synthetic noisy problem.

Setup. The settings of the experiment are generally the same as the synthetic experiment in He et al. [2024]. We consider the following noisy linear regression problem.

$$\min_{X \in \mathbb{R}^{n \times n}} f(x) \triangleq \frac{1}{2} \|AX\|_{\mathrm{F}}^2 + \langle B, X \rangle, \quad \nabla f(X; \xi) = \nabla f(X) + \xi \sigma C,$$

where $A = \begin{bmatrix} I_{n-r} & 0 \end{bmatrix} \in \mathbb{R}^{(n-r) \times n}$, $B = \begin{bmatrix} D & 0 \\ 0 & 0 \end{bmatrix} \in \mathbb{R}^{n \times n}$ with $D \in \mathbb{R}^{(n-r) \times (n-r)}$ a Gaussian random matrix, $C = \begin{bmatrix} 0 & 0 \\ 0 & I_r \end{bmatrix} \in \mathbb{R}^{n \times n}$, ξ is a random variable with probability 0.5 to be 1 and probability 0.5 to be 0, and σ is a constant controlling the noise level. It is straightforward to verify that this is a smooth and convex optimization problem, with bounded gradient variance.

In our experiment, we specifically set $n = 20$, $r = 12$, $\sigma = 100$ to construct a small-scale but noisy problem. For the vanilla (biased) GaLore Muon algorithm, we set the projection rank to be 12 as well. For GUM, we set $r = 2$ and $q_{t,\ell} = 0.5$. We can see that in this case, the memory footprints of the two algorithms are the same.

Results. The convergence result is shown in Figure 1. We adjust the minimum loss to 0 to better visualize the difference. As we can see, GaLore fails to converge at all, while GUM converges to a comparable accuracy with the full-parameter Muon baseline. The experiment shows a clear benefit of the unbiased method, at least in noisy settings.

Here is a more detailed analysis of why these conditions lead to GaLore's failure. In this synthetic problem, the noise level is set to be large and has rank $r = 12$, which is equal to the projection rank of GaLore. Since the noise is in a dominant position, every time the r largest singular values of the stochastic gradient

Table 1: **Space complexity** comparison between GaLore and GUM for a block $W \in \mathbb{R}^{m \times m}$ with $r' < r \leq m$ respectively. GUM uses a full-rank update with probability $q \in [0, 1]$, where the memory GUM has the same memory consumption when $q = 2(r - r')/(m - r')$.

Method	Space Complexity
GaLore	$\mathcal{O}(2mr)$
GUM	$\mathcal{O}((2-q)mr' + qm^2)$
SFT	$\mathcal{O}(m^2)$

$\nabla f(X; \xi)$ come from the noise, so do the corresponding singular vectors and the GaLore projection matrix. This meaningless projection makes the training process not even take a single effective step towards solving the problem. Therefore, this synthetic experiment shows an extreme case in which GaLore can fail when the gradient noise is large. Also, the experiment shows that GUM fixes the non-convergence problem with the same memory cost as GaLore-Muon.

5.2 LLM Fine-tuning Settings

To verify the empirical effectiveness of the proposed algorithm in practice, we compare GUM with GaLore in LLM fine-tuning settings.

Setup. The performance of the fine-tuned models is evaluated on two types of tasks: 1) IFEval [Zhou et al., 2023], an instruction-following benchmark that assesses models' adherence to explicit, verifiable instructions, and 2) GSM8K [Cobbe et al., 2021a], a mathematical reasoning benchmark that evaluates models' problem-solving skills in grad-school level math questions.

For model choices, LLaMA3-8B [Grattafiori et al., 2024b], Qwen2.5-7B [Qwen et al., 2025], and Gemma2-9B [Team et al., 2024] are adopted, which are commonly used in practical applications.

For training datasets, GPT-4-LLM is adopted on the instruction-following tasks of IFEval, which consists of 54.6K high-quality GPT-4-generated instruction-response pairs across various instruction categories. As for the mathematical reasoning task of GSM8K, a 2K-sized high-quality mixture [*] from DART-Math [Tong et al., 2024], Ultra-Interact [Yuan et al., 2024], MathInstruct [Yue et al., 2023], and Orca-Math [Mitra et al., 2024] is employed, which allows strong models such as Qwen-2.5-7B to still obtain reasonable improvements after fine-tuning.

---

[*]The dataset is from `https://huggingface.co/datasets/HanningZhang/scalebio_distill_qwen_math`, generated using the same setting as Appendix A.2 of [Pan et al., 2025].

Table 2: **LLM Fine-tuning Results.** Trained models are evaluated on IFEval (instruction-following) and GSM8K (mathematical reasoning). All experiments are conducted on a single H100 GPU.

Model	Memory Efficient	Method	IFEval		GSM8K
			Prompt-level Strict-Accuracy	Prompt-level Loose-Accuracy	Accuracy
LLaMA-3-8B	✗	FT-AdamW	23.66	25.14	57.39
		FT-Muon	23.11	26.06	57.65
	✓	GaLore	21.07	22.74	57.38
		Fira	21.81	23.73	56.41
		GUM	**22.37**	**24.03**	**58.45**
Qwen-2.5-7B	✗	FT-AdamW	35.12	39.74	85.75
		FT-Muon	34.38	39.19	85.90
	✓	GaLore	33.09	37.71	86.28
		Fira	32.35	36.04	86.81
		GUM	**33.46**	**38.82**	**86.81**
Gemma-2-9B	✗	FT-AdamW	OOM	OOM	OOM
		FT-Muon	28.47	32.16	76.92
	✓	GaLore	30.31	33.64	77.18
		Fira	29.21	33.64	75.44
		GUM	**33.27**	**36.60**	**77.48**

For hyperparameters, we adopt a rank of 512 for GaLore and 2 + 128 for GUM. The baselines include Full-parameter Training with Muon [Jordan et al., 2024] (FT-Muon), Full-parameter Training with AdamW [Loshchilov and Hutter, 2019] (FT-AdamW), and Gradient Low-Rank Projection (GaLore) [Zhao et al., 2024], where further details are available in Appendix C.

Memory Efficiency. We conducted peak GPU memory experiments to evaluate GUM's memory efficiency, demonstrating its comparable or reduced memory footprint relative to GaLore. Specifically, we focus on two key hyperparameters: the rank and the number of selected layers for full-rank updates in GUM. To ensure a fair comparison, all methods used a consistent mini-batch size of 1, without employing additional GPU memory-saving techniques such as offloading [Ren et al., 2021] or flash attention [Dao et al., 2022, Dao, 2024].

As shown in Table 3, the GUM configuration reaches comparable or better memory consumption than GaLore. This improvement is not limited to a single case; consistent memory savings are observed across multiple model architectures.

Table 3: **Peak GPU memory usage** across different model architectures and configurations, emphasizing the variations among them. As specified in the table, the GUM configuration 2 + 128 involves updating two layers with full-rank gradients, while all other layers are updated with low-rank gradients of rank $r = 128$.

Model	GaLore	GUM Layers + Rank	
	512	4 + 128	2 + 128
LLaMA-3-8B	42G	41G	**40G**
Qwen-2.5-7B	41G	40G	**39G**
Gemma-2-9B	47G	46G	**44G**

Results. As shown in Table 2, GUM consistently outperforms GaLore in both tasks, highlighting its robustness and general effectiveness.

A closer look at GSM8K results reveals that GUM achieves notable improvements and even outperforms full-parameter training methods, suggesting its strength in enhancing reasoning capabilities. In Section 5.4, it will be revealed that this improvement is very likely to have originated from its improvements in memorization, especially when the learned activations are required to be long-tailed.

Table 4: **LLM Pre-training Results.** Trained models are evaluated on seven widely adopted commonsense reasoning tasks. All experiments are conducted on H100 GPUs.

Model	Method	ARC-E	ARC-C	OBQA	HellaSwag	PIQA	SIQA	Winogrande	Avg.
LLaMA-60M	AdamW	32.87	17.92	12.68	26.70	58.87	35.88	50.12	33.58
	Muon	36.45	17.92	12.88	26.89	59.79	35.82	51.22	34.42
	GaLore	35.35	17.92	12.47	26.74	59.63	35.62	49.88	33.94
	Fira	35.02	18.94	12.27	26.75	58.71	36.24	50.28	34.03
	GUM	36.28	17.41	13.68	26.70	60.12	36.54	51.85	**34.65**
LLaMA-130M	AdamW	37.08	18.86	13.48	27.04	59.14	36.18	51.07	34.69
	Muon	38.34	18.00	13.08	27.67	62.68	37.00	49.33	35.16
	GaLore	36.49	18.00	13.28	27.08	60.34	35.36	50.20	34.39
	Fira	26.01	19.54	12.27	26.13	53.65	34.19	49.80	31.66
	GUM	38.01	18.34	14.69	27.32	61.26	36.44	52.49	**35.51**
LLaMA-350M	AdamW	44.02	18.77	14.08	30.04	64.42	37.97	50.51	37.12
	Muon	44.91	18.69	17.10	31.05	65.72	37.87	51.93	38.18
	GaLore	43.10	18.52	14.89	29.09	62.19	37.10	52.01	36.58
	Fira	42.38	18.77	15.49	29.27	63.00	37.97	51.85	36.96
	GUM	44.44	19.80	15.69	29.28	64.53	38.13	51.38	37.42

5.3 LLM Pre-training Settings

To provide stronger evidence for validating the effectiveness of GUM, a standard pre-training setting is introduced to compare different training methods' performance.

Setup. To evaluate the improvements in commonsense reasoning, the following downstream tasks are employed: ARC [Clark et al., 2018], OpenBookQA [Mihaylov et al., 2018a], HellaSwag Zellers et al. [2019a], PIQA [Bisk et al., 2020], SIQA [Sap et al., 2019], and WinoGrande [Sakaguchi et al., 2021a], which are common choices for LLM pre-training [Hoffmann et al., 2022a, Groeneveld et al., 2024, Zhang et al., 2024b]. For model choice, following the standard setting in Zhao et al. [2024], the experiments covered three model sizes—60M, 130M, and 350M parameters of LLaMA. For training datasets, we employ the widely-used C4 corpus [Raffel et al., 2023] under configurations guided by the Chinchilla scaling law [Hoffmann et al., 2022b]: 1.5B tokens for 60M, 2B tokens for 130M, and 7B tokens for 350M. For baselines, in addition to methods in Section 5.2, we include Fira [Chen et al., 2024], an optimizer designed to achieve full-rank training under low-rank constraints for improved efficiency. Further details are available in Appendix C.3.

Results. The performance comparison presented in Table 4 clearly indicates that GUM achieves consistently better results than GaLore and, more surprisingly, even full-parameter training methods like AdamW and Muon. This improvement can largely be attributed to the unbiased low-rank update mechanism employed in GUM. The mechanism captures long-tailed gradient updates distributed across layers and thereby enhances model memorization.

5.4 Understanding the Effect of Layerwise Sampling

In this section, we investigate the underlying reason why the proposed algorithm of GUM can yield empirical improvements over GaLore. In short, GUM's high-rank gradient update leads to a more uniform singular value distribution in model parameters, which further results in more evenly distributed activations for input samples. This implies the long-tailed knowledge is better preserved in GUM-trained models, yielding better memorization.

Setup. We adopt the model of LLaMA-130M and benchmark of ARC-E [Clark et al., 2018], while keeping other settings the same as in Section 5.3.

Results. As shown in Figure 2, the overall stable ranks $\mathbb{E}\left[\|M\|_F^2/\|M\|_2^2\right]$ of GaLore and GUM are positively correlated with their performance in ARC-E, which provides direct evidence that higher stable ranks are generally beneficial for improving commonsense reasoning.

On top of that, it is observed in Figure 3 that GUM not only improves the overall stable rank of the trained model, but also shapes a set of more evenly distributed singular values in trained models, which further leads to more long-tail distributed activation across all modules. This provides indirect evidence and an intuitive explanation for the performance improvements in ARC-E: instead of overusing a low-dimensional space or a
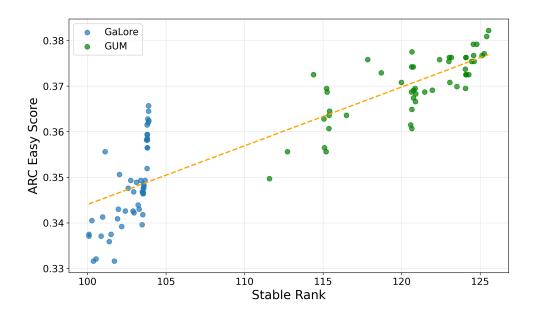
Figure 2: **Higher Stable Rank → Better Performance.** A positive correlation is observed between the overall stable rank $\mathbb{E}\left[\|M\|_F^2/\|M\|_2^2\right]$ and ARC Easy score. Each dot represents a checkpoint during pre-training after 1,000 steps, saved every 20 steps.

limited number of modules, GUM-trained models demonstrate a tendency to evenly distribute knowledge across all dimensions and modules, implying better memorization. Additional evidence is available in Appendix D.2.
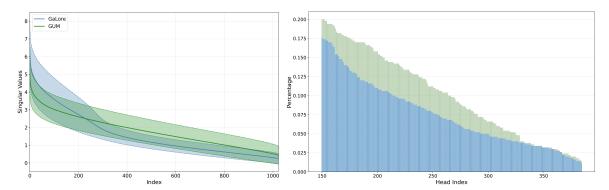

Figure 3: **Left: Updates → Weights**: Singular value distribution across layers of GaLore and GUM, where GUM demonstrates a more even and long-tailed distribution of singular values. **Right: Weights → Activations**: Tail distribution of modules that contain salient activations, where salient activations are defined as activations with top-k ($k = 10,000$) attention scores over all modules. Randomly sampled 1K inputs from the C4 corpus are utilized as prompts. Blue parts correspond to GaLore's tail distribution, while green parts stand for GUM's further increase on top of GaLore.

6   Conclusions

In this paper, we investigate the debiasing technique of layerwise sampling for memory-efficient LLM training, whose combination with GaLore restores the theoretical convergence properties of full-parameter training. Our proposed algorithm, GUM, demonstrates that it is possible to achieve provable convergence in low-rank optimization without impairing its empirical performance and memory efficiency. Further analysis shows that the empirical gains are brought by the inherent high-rank updates, which lead to a higher overall stable rank and more uniformly distributed singular values in model parameters, yielding more long-tailed activation patterns and implying better memorization.

Ethics Statement

After carefully reviewing the ethical regulations of the conference, to the best of our knowledge, this work does not present any foreseeable ethical concerns. No negative societal or ethical impacts are anticipated for the contribution of this work. The proposed algorithms are for general large language model training, and do not involve anything about human subjects, potentially harmful insights, potential conflicts of interest and sponsorship, discrimination/bias/fairness concerns, privacy and security issues, legal compliance, or research integrity issues.

Reproducibility Statement

We have made efforts to ensure that our work is reproducible, with details provided in Section 5 and Appendix C.

References

Keller Jordan, Yuchen Jin, Vlado Boza, Jiacheng You, Franz Cesista, Laker Newhouse, and Jeremy Bernstein. Muon: An optimizer for hidden layers in neural networks, 2024. URL https://kellerjordan.github.io/posts/muon/.

Long Ouyang, Jeffrey Wu, Xu Jiang, Diogo Almeida, Carroll Wainwright, Pamela Mishkin, Chong Zhang, Sandhini Agarwal, Katarina Slama, Alex Ray, John Schulman, Jacob Hilton, Fraser Kelton, Luke Miller, Maddie Simens, Amanda Askell, Peter Welinder, Paul F Christiano, Jan Leike, and Ryan Lowe. Training language models to follow instructions with human feedback. In S. Koyejo, S. Mohamed, A. Agarwal, D. Belgrave, K. Cho, and A. Oh, editors, *Advances in Neural Information Processing Systems*, volume 35, pages 27730–27744. Curran Associates, Inc., 2022.

Aaron Grattafiori, Abhimanyu Dubey, Abhinav Jauhri, Abhinav Pandey, Abhishek Kadian, Ahmad Al-Dahle, Aiesha Letman, Akhil Mathur, Alan Schelten, Alex Vaughan, et al. The llama 3 herd of models. *arXiv preprint arXiv:2407.21783*, 2024a.

Daya Guo, Dejian Yang, Haowei Zhang, Junxiao Song, Ruoyu Zhang, Runxin Xu, Qihao Zhu, Shirong Ma, Peiyi Wang, Xiao Bi, et al. Deepseek-r1: Incentivizing reasoning capability in llms via reinforcement learning. *arXiv preprint arXiv:2501.12948*, 2025.

Yujia Qin, Yining Ye, Junjie Fang, Haoming Wang, Shihao Liang, Shizuo Tian, Junda Zhang, Jiahao Li, Yunxin Li, Shijue Huang, et al. Ui-tars: Pioneering automated gui interaction with native agents. *arXiv preprint arXiv:2501.12326*, 2025.

Jiawei Zhao, Zhenyu Zhang, Beidi Chen, Zhangyang Wang, Anima Anandkumar, and Yuandong Tian. Galore: Memory-efficient llm training by gradient low-rank projection. *arXiv preprint arXiv:2403.03507*, 2024.

Diederik P Kingma and Jimmy Ba. Adam: A method for stochastic optimization. *arXiv preprint arXiv:1412.6980*, 2014.

Aashiq Muhamed, Oscar Li, David Woodruff, Mona Diab, and Virginia Smith. Grass: Compute efficient low-memory llm training with structured sparse gradients. *arXiv preprint arXiv:2406.17660*, 2024.

Luoming Zhang, Zhenyu Lou, Yangwei Ying, Cheng Yang, and Hong Zhou. Efficient fine-tuning of large language models via a low-rank gradient estimator. *Applied Sciences*, 15(1):82, 2024a.

Yutong He, Pengrui Li, Yipeng Hu, Chuyan Chen, and Kun Yuan. Subspace optimization for large language models with convergence guarantees. *arXiv preprint arXiv:2410.11289*, 2024.

Jia-Hong Huang, Yixian Shen, Hongyi Zhu, Stevan Rudinac, and Evangelos Kanoulas. Gradient weight-normalized low-rank projection for efficient llm training. In *Proceedings of the AAAI Conference on Artificial Intelligence*, volume 39, pages 24123–24131, 2025.

Ning Ding, Yujia Qin, Guang Yang, Fuchao Wei, Zonghan Yang, Yusheng Su, Shengding Hu, Yulin Chen, Chi-Min Chan, Weize Chen, et al. Delta tuning: A comprehensive study of parameter efficient methods for pre-trained language models. *arXiv preprint arXiv:2203.06904*, 2022.

Rui Pan, Xiang Liu, Shizhe Diao, Renjie Pi, Jipeng Zhang, Chi Han, and Tong Zhang. Lisa: layerwise importance sampling for memory-efficient large language model fine-tuning. *Advances in Neural Information Processing Systems*, 37:57018–57049, 2024.

Edward J Hu, yelong shen, Phillip Wallis, Zeyuan Allen-Zhu, Yuanzhi Li, Shean Wang, Lu Wang, and Weizhu Chen. LoRA: Low-rank adaptation of large language models. In *International Conference on Learning Representations*, 2022. URL `https://openreview.net/forum?id=nZeVKeeFYf9`.

Vladislav Lialin, Namrata Shivagunde, Sherin Muckatira, and Anna Rumshisky. Relora: High-rank training through low-rank updates, 2023.

Demi Guo, Alexander M Rush, and Yoon Kim. Parameter-efficient transfer learning with diff pruning. *arXiv preprint arXiv:2012.07463*, 2020.

Yi-Lin Sung, Varun Nair, and Colin A Raffel. Training neural networks with fixed sparse masks. *Advances in Neural Information Processing Systems*, 34:24193–24205, 2021.

Alan Ansell, Edoardo Maria Ponti, Anna Korhonen, and Ivan Vulić. Composable sparse fine-tuning for cross-lingual transfer. *arXiv preprint arXiv:2110.07560*, 2021.

Sarkar Snigdha Sarathi Das, Ranran Haoran Zhang, Peng Shi, Wenpeng Yin, and Rui Zhang. Unified low-resource sequence labeling by sample-aware dynamic sparse finetuning. *arXiv preprint arXiv:2311.03748*, 2023.

Xinxin Liu, Aaron Thomas, Cheng Zhang, Jianyi Cheng, Yiren Zhao, and Xitong Gao. Refining salience-aware sparse fine-tuning strategies for language models. *arXiv preprint arXiv:2412.13488*, 2024a.

Dan Alistarh, Demjan Grubic, Jerry Li, Ryota Tomioka, and Milan Vojnovic. Qsgd: Communication-efficient sgd via gradient quantization and encoding. *Advances in neural information processing systems*, 30, 2017.

Ananda Theertha Suresh, X Yu Felix, Sanjiv Kumar, and H Brendan McMahan. Distributed mean estimation with limited communication. In *International conference on machine learning*, pages 3329–3337. PMLR, 2017.

Bokun Wang, Mher Safaryan, and Peter Richtárik. Theoretically better and numerically faster distributed optimization with smoothness-aware quantization techniques. *Advances in Neural Information Processing Systems*, 35:9841–9852, 2022.

Jianqiao Wangni, Jialei Wang, Ji Liu, and Tong Zhang. Gradient sparsification for communication-efficient distributed optimization. *Advances in Neural Information Processing Systems*, 31, 2018.

Sebastian U Stich, Jean-Baptiste Cordonnier, and Martin Jaggi. Sparsified sgd with memory. *Advances in neural information processing systems*, 31, 2018.

Hongyi Wang, Scott Sievert, Shengchao Liu, Zachary Charles, Dimitris Papailiopoulos, and Stephen Wright. Atomo: Communication-efficient learning via atomic sparsification. *Advances in neural information processing systems*, 31, 2018.

Xi Chen, Kaituo Feng, Changsheng Li, Xunhao Lai, Xiangyu Yue, Ye Yuan, and Guoren Wang. Fira: Can we achieve full-rank training of llms under low-rank constraint?, 2024. URL `https://arxiv.org/abs/2410.01623`.

Jingyuan Liu, Jianlin Su, Xingcheng Yao, Zhejun Jiang, Guokun Lai, Yulun Du, Yidao Qin, Weixin Xu, Enzhe Lu, Junjie Yan, et al. Muon is scalable for llm training. *arXiv preprint arXiv:2502.16982*, 2025a.

Team Kimi. Kimi-vl technical report. *arXiv preprint arXiv:2504.07491*, 2025.

Kang An, Yuxing Liu, Rui Pan, Shiqian Ma, Donald Goldfarb, and Tong Zhang. Asgo: Adaptive structured gradient optimization. *arXiv preprint arXiv:2503.20762*, 2025.

Jiaxiang Li and Mingyi Hong. A note on the convergence of muon and further. *arXiv preprint arXiv:2502.02900*, 2025.

Jeremy Bernstein, Yu-Xiang Wang, Kamyar Azizzadenesheli, and Animashree Anandkumar. signsgd: Compressed optimisation for non-convex problems. In *International Conference on Machine Learning*, pages 560–569. PMLR, 2018.

Michael Crawshaw, Mingrui Liu, Francesco Orabona, Wei Zhang, and Zhenxun Zhuang. Robustness to unbounded smoothness of generalized signsgd. *Advances in neural information processing systems*, 35: 9955–9968, 2022.

Yuxing Liu, Rui Pan, and Tong Zhang. Adagrad under anisotropic smoothness. *arXiv preprint arXiv:2406.15244*, 2024b.

Jeffrey Zhou, Tianjian Lu, Swaroop Mishra, Siddhartha Brahma, Sujoy Basu, Yi Luan, Denny Zhou, and Le Hou. Instruction-following evaluation for large language models, 2023. URL https://arxiv.org/abs/2311.07911.

Karl Cobbe, Vineet Kosaraju, Mohammad Bavarian, Mark Chen, Heewoo Jun, Lukasz Kaiser, Matthias Plappert, Jerry Tworek, Jacob Hilton, Reiichiro Nakano, Christopher Hesse, and John Schulman. Training verifiers to solve math word problems, 2021a.

Aaron Grattafiori, Abhimanyu Dubey, Abhinav Jauhri, Abhinav Pandey, Abhishek Kadian, Ahmad Al-Dahle, Aiesha Letman, Akhil Mathur, Alan Schelten, Alex Vaughan, Amy Yang, Angela Fan, Anirudh Goyal, Anthony Hartshorn, and et al. The llama 3 herd of models, 2024b. URL https://arxiv.org/abs/2407.21783.

Qwen, :, An Yang, Baosong Yang, Beichen Zhang, Binyuan Hui, Bo Zheng, Bowen Yu, Chengyuan Li, Dayiheng Liu, Fei Huang, Haoran Wei, Huan Lin, Jian Yang, Jianhong Tu, Jianwei Zhang, Jianxin Yang, Jiaxi Yang, Jingren Zhou, Junyang Lin, Kai Dang, Keming Lu, Keqin Bao, Kexin Yang, Le Yu, Mei Li, Mingfeng Xue, Pei Zhang, Qin Zhu, Rui Men, Runji Lin, Tianhao Li, Tianyi Tang, Tingyu Xia, Xingzhang Ren, Xuancheng Ren, Yang Fan, Yang Su, Yichang Zhang, Yu Wan, Yuqiong Liu, Zeyu Cui, Zhenru Zhang, and Zihan Qiu. Qwen2.5 technical report, 2025. URL https://arxiv.org/abs/2412.15115.

Gemma Team, Morgane Riviere, Shreya Pathak, Pier Giuseppe Sessa, Cassidy Hardin, Surya Bhupatiraju, Léonard Hussenot, Thomas Mesnard, Bobak Shahriari, Alexandre Ramé, Johan Ferret, Peter Liu, Pouya Tafti, Abe Friesen, Michelle Casbon, Sabela Ramos, Ravin Kumar, Charline Le Lan, Sammy Jerome, Anton Tsitsulin, Nino Vieillard, Piotr Stanczyk, Sertan Girgin, Nikola Momchev, Matt Hoffman, Shantanu Thakoor, Jean-Bastien Grill, Behnam Neyshabur, Olivier Bachem, Alanna Walton, Aliaksei Severyn, Alicia Parrish, Aliya Ahmad, Allen Hutchison, Alvin Abdagic, Amanda Carl, Amy Shen, Andy Brock, Andy Coenen, Anthony Laforge, Antonia Paterson, Ben Bastian, Bilal Piot, Bo Wu, Brandon Royal, Charlie Chen, Chintu Kumar, Chris Perry, Chris Welty, Christopher A. Choquette-Choo, Danila Sinopalnikov, David Weinberger, Dimple Vijaykumar, Dominika Rogozińska, Dustin Herbison, Elisa Bandy, Emma Wang, Eric Noland, Erica Moreira, Evan Senter, Evgenii Eltyshev, Francesco Visin, Gabriel Rasskin, Gary Wei, Glenn Cameron, Gus Martins, Hadi Hashemi, Hanna Klimczak-Plucińska, Harleen Batra, Harsh Dhand, Ivan Nardini, Jacinda Mein, Jack Zhou, James Svensson, Jeff Stanway, Jetha Chan, Jin Peng Zhou, Joana Carrasqueira, Joana Iljazi, Jocelyn Becker, Joe Fernandez, Joost van Amersfoort, Josh Gordon, Josh Lipschultz, Josh Newlan, Ju yeong Ji, Kareem Mohamed, Kartikeya Badola, Kat Black, Katie Millican, Keelin McDonell, Kelvin Nguyen, Kiranbir Sodhia, Kish Greene, Lars Lowe Sjoesund, Lauren Usui, Laurent Sifre, Lena Heuermann, Leticia Lago, Lilly McNealus, Livio Baldini Soares, Logan Kilpatrick, Lucas Dixon, Luciano Martins, Machel Reid, Manvinder Singh, Mark Iverson, Martin Görner, Mat Velloso, Mateo Wirth, Matt Davidow, Matt Miller, Matthew Rahtz, Matthew Watson, Meg Risdal, Mehran Kazemi, Michael Moynihan, Ming Zhang, Minsuk Kahng, Minwoo Park, Mofi Rahman, Mohit Khatwani, Natalie Dao, Nenshad Bardoliwalla, Nesh Devanathan, Neta Dumai, Nilay Chauhan, Oscar Wahltinez, Pankil Botarda, Parker Barnes, Paul Barham, Paul Michel, Pengchong Jin, Petko Georgiev, Phil Culliton, Pradeep Kuppala, Ramona Comanescu, Ramona Merhej, Reena Jana, Reza Ardeshir Rokni, Rishabh Agarwal, Ryan Mullins, Samaneh Saadat, Sara Mc Carthy, Sarah Cogan, Sarah Perrin, Sébastien M. R. Arnold, Sebastian Krause, Shengyang Dai, Shruti Garg, Shruti Sheth, Sue Ronstrom, Susan Chan, Timothy Jordan, Ting Yu, Tom Eccles, Tom Hennigan, Tomas Kocisky, Tulsee Doshi, Vihan Jain, Vikas Yadav, Vilobh Meshram, Vishal Dharmadhikari, Warren Barkley, Wei Wei, Wenming Ye, Woohyun Han, Woosuk Kwon, Xiang Xu, Zhe Shen, Zhitao Gong, Zichuan Wei, Victor Cotruta, Phoebe Kirk, Anand Rao, Minh Giang, Ludovic Peran, Tris Warkentin, Eli Collins, Joelle Barral, Zoubin Ghahramani, Raia Hadsell, D. Sculley, Jeanine Banks, Anca Dragan, Slav Petrov, Oriol Vinyals, Jeff Dean, Demis Hassabis,

Koray Kavukcuoglu, Clement Farabet, Elena Buchatskaya, Sebastian Borgeaud, Noah Fiedel, Armand Joulin, Kathleen Kenealy, Robert Dadashi, and Alek Andreev. Gemma 2: Improving open language models at a practical size, 2024. URL `https://arxiv.org/abs/2408.00118`.

Rui Pan, Dylan Zhang, Hanning Zhang, Xingyuan Pan, Minrui Xu, Jipeng Zhang, Renjie Pi, Xiaoyu Wang, and Tong Zhang. ScaleBiO: Scalable bilevel optimization for LLM data reweighting. In *Proceedings of the 63rd Annual Meeting of the Association for Computational Linguistics*, pages 31959–31982, 2025.

Yuxuan Tong, Xiwen Zhang, Rui Wang, Ruidong Wu, and Junxian He. Dart-math: Difficulty-aware rejection tuning for mathematical problem-solving. 2024. URL `https://arxiv.org/abs/2407.13690`.

Lifan Yuan, Ganqu Cui, Hanbin Wang, Ning Ding, Xingyao Wang, Jia Deng, Boji Shan, Huimin Chen, Ruobing Xie, Yankai Lin, Zhenghao Liu, Bowen Zhou, Hao Peng, Zhiyuan Liu, and Maosong Sun. Advancing llm reasoning generalists with preference trees, 2024.

Xiang Yue, Xingwei Qu, Ge Zhang, Yao Fu, Wenhao Huang, Huan Sun, Yu Su, and Wenhu Chen. Mammoth: Building math generalist models through hybrid instruction tuning. *arXiv preprint arXiv:2309.05653*, 2023.

Arindam Mitra, Hamed Khanpour, Corby Rosset, and Ahmed Awadallah. Orca-math: Unlocking the potential of slms in grade school math, 2024.

Ilya Loshchilov and Frank Hutter. Decoupled weight decay regularization, 2019. URL `https://arxiv.org/abs/1711.05101`.

Jie Ren, Samyam Rajbhandari, Reza Yazdani Aminabadi, Olatunji Ruwase, Shuangyan Yang, Minjia Zhang, Dong Li, and Yuxiong He. Zero-offload: Democratizing billion-scale model training, 2021. URL `https://arxiv.org/abs/2101.06840`.

Tri Dao, Daniel Y. Fu, Stefano Ermon, Atri Rudra, and Christopher Ré. FlashAttention: Fast and memory-efficient exact attention with IO-awareness. In *Advances in Neural Information Processing Systems*, 2022.

Tri Dao. Flashattention-2: Faster attention with better parallelism and work partitioning. In *The Twelfth International Conference on Learning Representations*, 2024. URL `https://openreview.net/forum?id=mZn2Xyh9Ec`.

Peter Clark, Isaac Cowhey, Oren Etzioni, Tushar Khot, Ashish Sabharwal, Carissa Schoenick, and Oyvind Tafjord. Think you have solved question answering? try ARC, the AI2 reasoning challenge. In *Proceedings of the 2018 Conference of the North American Chapter of the Association for Computational Linguistics: Human Language Technologies*, New Orleans, Louisiana, May 2018. Association for Computational Linguistics. doi: 10.18653/v1/N18-1074. URL `https://arxiv.org/abs/1803.05457`.

Todor Mihaylov, Peter Clark, Tushar Khot, and Ashish Sabharwal. Can a suit of armor conduct electricity? a new dataset for open book question answering. In *Proceedings of the 2018 Conference on Empirical Methods in Natural Language Processing*, pages 2381–2391, Brussels, Belgium, October-November 2018a. Association for Computational Linguistics. doi: 10.18653/v1/D18-1260. URL `https://aclanthology.org/D18-1260/`.

Rowan Zellers, Ari Holtzman, Yonatan Bisk, Ali Farhadi, and Yejin Choi. Hellaswag: Can a machine really finish your sentence? In *Proceedings of the 57th Annual Meeting of the Association for Computational Linguistics*, pages 4791–4800, Florence, Italy, July 2019a. Association for Computational Linguistics. doi: 10.18653/v1/P19-1472. URL `https://aclanthology.org/P19-1472/`.

Yonatan Bisk, Rowan Zellers, Omer Yakhini, and Yejin Choi. Piqa: Reasoning about physical commonsense in natural language. *arXiv preprint*, 2020. URL `https://arxiv.org/abs/1911.11641`.

Maarten Sap, Hannah Rashkin, Derek Chen, Ronan Le Bras, and Yejin Choi. Social IQa: Commonsense reasoning about social interactions. In *Proceedings of the 2019 Conference on Empirical Methods in Natural Language Processing and the 9th International Joint Conference on Natural Language Processing (EMNLP-IJCNLP)*, pages 4463–4473, Hong Kong, China, November 2019. Association for Computational Linguistics. doi: 10.18653/v1/D19-1454. URL `https://aclanthology.org/D19-1454/`.

Keisuke Sakaguchi, Ronan Le Bras, Chandra Bhagavatula, and Yejin Choi. Winogrande: An adversarial winograd schema challenge at scale. *Communications of the ACM*, 64(9):99–106, September 2021a. doi: 10.1145/3474381.

Jordan Hoffmann, Sebastian Borgeaud, Arthur Mensch, Elena Buchatskaya, Trevor Cai, Eliza Rutherford, Diego de Las Casas, Lisa Anne Hendricks, Johannes Welbl, Aidan Clark, et al. Training compute-optimal large language models. *arXiv preprint arXiv:2203.15556*, 2022a.

Dirk Groeneveld, Iz Beltagy, Pete Walsh, Akshita Bhagia, Rodney Kinney, Oyvind Tafjord, Ananya Harsh Jha, Hamish Ivison, Ian Magnusson, Yizhong Wang, et al. Olmo: Accelerating the science of language models. *arXiv preprint arXiv:2402.00838*, 2024.

Peiyuan Zhang, Guangtao Zeng, Tianduo Wang, and Wei Lu. Tinyllama: An open-source small language model, 2024b.

Colin Raffel, Noam Shazeer, Adam Roberts, Katherine Lee, Sharan Narang, Michael Matena, Yanqi Zhou, Wei Li, and Peter J. Liu. Exploring the limits of transfer learning with a unified text-to-text transformer, 2023. URL https://arxiv.org/abs/1910.10683.

Jordan Hoffmann, Sebastian Borgeaud, Arthur Mensch, Elena Buchatskaya, Trevor Cai, Eliza Rutherford, Diego de Las Casas, Lisa Anne Hendricks, Johannes Welbl, Aidan Clark, Tom Hennigan, Eric Noland, Katie Millican, George van den Driessche, Bogdan Damoc, Aurelia Guy, Simon Osindero, Karen Simonyan, Erich Elsen, Jack W. Rae, Oriol Vinyals, and Laurent Sifre. Training compute-optimal large language models, 2022b. URL https://arxiv.org/abs/2203.15556.

Amrutha Varshini Ramesh, Vignesh Ganapathiraman, Issam H Laradji, and Mark Schmidt. Blockllm: Memory-efficient adaptation of llms by selecting and optimizing the right coordinate blocks. *arXiv preprint arXiv:2406.17296*, 2024.

Ashok Cutkosky and Harsh Mehta. Momentum improves normalized sgd. In *International conference on machine learning*, pages 2260–2268. PMLR, 2020.

Tao Sun, Qingsong Wang, Dongsheng Li, and Bao Wang. Momentum ensures convergence of signsgd under weaker assumptions. In *International Conference on Machine Learning*, pages 33077–33099. PMLR, 2023.

Shizhe Diao, Rui Pan, Hanze Dong, Ka Shun Shum, Jipeng Zhang, Wei Xiong, and Tong Zhang. Lmflow: An extensible toolkit for finetuning and inference of large foundation models. *arXiv preprint arXiv:2306.12420*, 2023.

Rie Johnson and Tong Zhang. Accelerating stochastic gradient descent using predictive variance reduction. *Advances in neural information processing systems*, 26, 2013.

Deanna Needell, Nathan Srebro, and Rachel Ward. Stochastic gradient descent, weighted sampling, and the randomized kaczmarz algorithm. *Advances in neural information processing systems*, 27, 2014.

Rong Ge, Zhize Li, Weiyao Wang, and Xiang Wang. Stabilized svrg: Simple variance reduction for nonconvex optimization. In *Conference on learning theory*, pages 1394–1448. PMLR, 2019a.

Yuchen Zhang and Lin Xiao. Stochastic primal-dual coordinate method for regularized empirical risk minimization. *Journal of Machine Learning Research*, 18(84):1–42, 2017.

Rong Ge, Sham M Kakade, Rahul Kidambi, and Praneeth Netrapalli. The step decay schedule: A near optimal, geometrically decaying learning rate procedure for least squares. *Advances in neural information processing systems*, 32, 2019b.

Rui Pan, Haishan Ye, and Tong Zhang. Eigencurve: Optimal learning rate schedule for sgd on quadratic objectives with skewed hessian spectrums. *arXiv preprint arXiv:2110.14109*, 2021.

Rui Pan, Yuxing Liu, Xiaoyu Wang, and Tong Zhang. Accelerated convergence of stochastic heavy ball method under anisotropic gradient noise. *arXiv preprint arXiv:2312.14567*, 2023.

Aaron Defazio, Xingyu Yang, Ahmed Khaled, Konstantin Mishchenko, Harsh Mehta, and Ashok Cutkosky. The road less scheduled. *Advances in Neural Information Processing Systems*, 37:9974–10007, 2024.

Yuxing Liu, Yuze Ge, Rui Pan, An Kang, and Tong Zhang. Theoretical analysis on how learning rate warmup accelerates convergence. *arXiv preprint arXiv:2509.07972*, 2025b.

Martin Arjovsky, Léon Bottou, Ishaan Gulrajani, and David Lopez-Paz. Invariant risk minimization. *arXiv preprint arXiv:1907.02893*, 2019.

Pierre Foret, Ariel Kleiner, Hossein Mobahi, and Behnam Neyshabur. Sharpness-aware minimization for efficiently improving generalization. *arXiv preprint arXiv:2010.01412*, 2020.

Yifan Hao, Xingyuan Pan, Hanning Zhang, Chenlu Ye, Rui Pan, and Tong Zhang. Understanding overadaptation in supervised fine-tuning: The role of ensemble methods. *arXiv preprint arXiv:2506.01901*, 2025.

Jacob Devlin, Ming-Wei Chang, Kenton Lee, and Kristina Toutanova. BERT: Pre-training of deep bidirectional transformers for language understanding. In Jill Burstein, Christy Doran, and Thamar Solorio, editors, *Proceedings of the 2019 Conference of the North American Chapter of the Association for Computational Linguistics: Human Language Technologies, Volume 1 (Long and Short Papers)*, pages 4171–4186, Minneapolis, Minnesota, June 2019. Association for Computational Linguistics. doi: 10.18653/v1/N19-1423. URL https://aclanthology.org/N19-1423.

Robin Rombach, Andreas Blattmann, Dominik Lorenz, Patrick Esser, and Björn Ommer. High-resolution image synthesis with latent diffusion models. In *Proceedings of the IEEE/CVF conference on computer vision and pattern recognition*, pages 10684–10695, 2022.

Rui Pan, Shizhe Diao, Jianlin Chen, and Tong Zhang. Extremebert: A toolkit for accelerating pretraining of customized bert. *arXiv preprint arXiv:2211.17201*, 2022.

Haotian Liu, Chunyuan Li, Qingyang Wu, and Yong Jae Lee. Visual instruction tuning. *Advances in neural information processing systems*, 36:34892–34916, 2023.

Albert Gu and Tri Dao. Mamba: Linear-time sequence modeling with selective state spaces. *arXiv preprint arXiv:2312.00752*, 2023.

Zijian Hu, Jipeng Zhang, Rui Pan, Zhaozhuo Xu, Shanshan Han, Han Jin, Alay Dilipbhai Shah, Dimitris Stripelis, Yuhang Yao, Salman Avestimehr, et al. Fox-1: Open small language model for cloud and edge. *arXiv preprint arXiv:2411.05281*, 2024.

Zihan Wang, Rui Pan, Jiarui Yao, Robert Csordas, Linjie Li, Lu Yin, Jiajun Wu, Tong Zhang, Manling Li, and Shiwei Liu. Chain-of-experts: Unlocking the communication power of mixture-of-experts models. *arXiv preprint arXiv:2506.18945*, 2025.

Siyuan Mu and Sen Lin. A comprehensive survey of mixture-of-experts: Algorithms, theory, and applications. *arXiv preprint arXiv:2503.07137*, 2025.

Mengzhou Xia, Tianyu Gao, Zhiyuan Zeng, and Danqi Chen. Sheared llama: Accelerating language model pre-training via structured pruning. *arXiv preprint arXiv:2310.06694*, 2023.

William Peebles and Saining Xie. Scalable diffusion models with transformers. In *Proceedings of the IEEE/CVF international conference on computer vision*, pages 4195–4205, 2023.

Karl Cobbe, Vineet Kosaraju, Mohammad Bavarian, Mark Chen, Heewoo Jun, Lukasz Kaiser, Matthias Plappert, Jerry Tworek, Jacob Hilton, Reiichiro Nakano, Christopher Hesse, and John Schulman. Training verifiers to solve math word problems, 2021b. URL https://arxiv.org/abs/2110.14168.

Rowan Zellers, Ari Holtzman, Yonatan Bisk, Ali Farhadi, and Yejin Choi. Hellaswag: Can a machine really finish your sentence? In *Proceedings of the 57th Annual Meeting of the Association for Computational Linguistics*, 2019b.

Jeffrey Li, Alex Fang, Georgios Smyrnis, Maor Ivgi, Matt Jordan, Samir Yitzhak Gadre, Hritik Bansal, Etash Guha, Sedrick Scott Keh, Kushal Arora, et al. Datacomp-lm: In search of the next generation of training sets for language models. *Advances in Neural Information Processing Systems*, 37:14200–14282, 2024.

Keisuke Sakaguchi, Ronan Le Bras, Chandra Bhagavatula, and Yejin Choi. Winogrande: An adversarial winograd schema challenge at scale. *Communications of the ACM*, 64(9):99–106, 2021b.

Todor Mihaylov, Peter Clark, Tushar Khot, and Ashish Sabharwal. Can a suit of armor conduct electricity? a new dataset for open book question answering. In *EMNLP*, 2018b.

Algorithm 3 An unbiased version of Algorithm 1

1: **Input:** $\{W_{0,\ell} \in \mathbb{R}^{m_\ell \times n_\ell}\}$ with each ℓ corresponding to the ℓ-th block of parameters, number of blocks N_L, sampling period K, projection rank r
2: **for** $t = 0$ **to** $T/K - 1$ **do**
3:     `delete_optimizer_states()`   ▷ Delete the optimizer states to clear memory
4:     Each block ℓ is sampled to do full-rank updates with probability $q_{t,\ell}$
5:     **for** $k = 0$ **to** $K - 1$ **do**
6:         **for** $\ell = 1$ **to** N_ℓ **do**
7:             $G_{t,k,\ell} = G(W_{tK+k-1,\ell})$ ▷ Obtain the gradient of the ℓ-th layer at W_t
8:             $P_{t,k,\ell} \leftarrow$ `get_projector()`   ▷ Obtain the projector $P_{t,k,\ell} \in \mathbb{R}^{m_\ell \times r}$
9:             $\tilde{G}_{t,k,\ell} = \begin{cases} \frac{1}{q_{t,\ell}}(I_{m_\ell} - P_{t,k,\ell}P_{t,k,\ell}^\top)G_{t,k,\ell}, & \text{if block } \ell \text{ is sampled to be full-rank} \\ \frac{1}{1-q_{t,\ell}}P_{t,k,\ell}^\top G_{t,k,\ell}, & \text{else} \end{cases}$
10:             $S_{t,k,\ell} \leftarrow$ `optimizer.update_state`$(\tilde{G}_{t,k,\ell})$ ▷ Run the base algorithm with $\tilde{G}_{t,k,\ell}$
11:             $W_{tK+k+1,\ell} = \begin{cases} W_{tK+k,\ell} - \eta S_{t,k,\ell}, & \text{if block } \ell \text{ is sampled to be full-rank} \\ W_{tK+k,\ell} - \eta P_{t,k,\ell}S_{t,k,\ell}, & \text{else} \end{cases}$
12:         **end for**
13:     **end for**
14: **end for**

A   A General Unbiased Low-Rank Gradient Method Paradigm

Here, we present our unbiased algorithm paradigm in Algorithm 3. The key idea of the algorithm is to compensate for biased errors introduced by the low-rank projection $P_t P_t^\top G_t$. To implement this while retaining memory efficiency, we refer to the main idea of LISA [Pan et al., 2024], which allows some of the blocks to be sampled uniformly with probability q in each period. This compensated full-rank updates use $G_t - P_t P_t^\top G_t$, while other blocks still do the original low-rank update. By carefully balancing the scaling constants for the two different updates, the biased low-rank term can be canceled out in expectation, resulting in an unbiased estimation of gradients across iterations. This unbiased version of the algorithm is presented in Algorithm 3.

In one training process, the algorithm contains separated periods just like the vanilla GaLore algorithm [Zhao et al., 2024] and LISA [Pan et al., 2024]. During each period t, each block of parameters is sampled to do full-rank updates with probability $q_{t,\ell}$. In each iteration k in the period, we first compute the projection matrix $P_{t,k,\ell}$. Note that a lot of strategies for selecting projection matrices and sampling importance can be applied here [Guo et al., 2020, Sung et al., 2021, Ansell et al., 2021, Das et al., 2023, Muhamed et al., 2024, Ramesh et al., 2024, Liu et al., 2024a]. Then, the blocks not sampled to do full-rank updates run basically the same low-rank update with Algorithm 1, while the full-rank blocks directly run the base optimizer with the compensated gradient $\tilde{G}_{t,k,\ell} = (I_m - P_{t,k,\ell}P_{t,k,\ell}^\top)G_{t,k,\ell}$.

We note that the proposed debiasing technique Algorithm 3 works generally when the following properties are satisfied:

- **Property I.** The columns of the low-rank projection matrix $P_t \in \mathbb{R}^{m \times r}$ with $r \leq m$ are orthonormal, i.e., $P_t^\top P_t = I_{r \times r}$.

- **Property II.** The projection and optimization updates are commutable, which means that

$$S_t = P_t \text{optimizer.update\_state}(\tilde{G}_t) = \text{optimizer.update\_state}(P_t \tilde{G}_t).$$

    Optimizers satisfying this property typically treat the update parameters as matrices instead of vectors, and only conduct matrix operations in the update. Two standard examples include SGD and Muon [Jordan et al., 2024].

If the two properties are satisfied, we can show that Algorithm 3 is unbiased compared to the base optimizer, since it is equivalent to running the base optimizer with an unbiased estimation of the gradient at each iteration.

Lemma 2 (Unbiased update of Algorithm 3). *When Property I and II are satisfied, a single iteration of Algorithm 3 for $W \in \mathbb{R}^{m \times n}$ is equivalent to*

$$S \leftarrow \text{optimizer.update\_state}(\hat{G})$$

$$W^+ = W - \eta S$$

with $\mathbb{E}[\hat{G}] = G \in \mathbb{R}^{m \times n}$, *where G denotes the gradient obtained at W.*

B Proofs of Section 3 and 4

B.1 Proof of Lemma 2 and 1

Proof of Lemma 2. A single step of Algorithm 3 writes:

$$\tilde{G} = \begin{cases} \frac{1}{q}(I - PP^\top)G, & \text{with probability } q \\ \frac{1}{1-q}P^\top G, & \text{with probability } 1 - q \end{cases}$$

$$S = \texttt{optimizer.update\_state}(\tilde{G})$$

$$W^+ = \begin{cases} W - \eta S, & \text{with probability } q \\ W - \eta PS, & \text{with probability } 1 - q \end{cases}$$

where G is the gradient at W and P is the projection matrix obtained at W. Based on the commutative property, we know that

$$W^+ = W - \eta PS = W - \eta \, \texttt{optimizer.update\_state}(P\tilde{G}),$$

which means that the update step is equivalent to

$$\hat{G} = \begin{cases} \frac{1}{q}(I - PP^\top)G, & \text{with probability } q \\ \frac{1}{1-q}PP^\top G, & \text{with probability } 1 - q \end{cases}$$

$$S = \texttt{optimizer.update\_state}(\hat{G})$$

$$W^+ = W - \eta S$$

Since we have $\hat{G}$ is an unbiased estimation of G:

$$\mathbb{E}[\hat{G}] = q \cdot \frac{1}{q}(I - PP^\top)G + (1 - q) \cdot \frac{1}{1 - q}PP^\top G = G,$$

we finish the proof that Algorithm 3 is unbiased compared to the base optimizer. $\square$

Proof of Lemma 1. Based on Lemma 2, we only need to prove that GUM satisfies the two properties to finish the proof of Lemma 1.

Property I. Denote the projection matrix at one specific iteration P. Since P is obtained from the SVD, we have $P \in \mathbb{R}^{m \times r}$ and $P^\top P = I_r$.

Property II. The base algorithm of GUM is Muon [Jordan et al., 2024]. To prove the commutative property, we only need to prove that the Newton-Schulz iteration is commutable with P. In each iteration of the Newton Schulz iteration $\texttt{NewtonSchulz}(X)$, we compute

$$X^+ = aX + bXX^\top X + cXX^\top XX^\top X,$$

where $a, b, c \in \mathbb{R}$ are absolute constants. Then consider $\texttt{NewtonSchulz}(PX)$, we get

$$X^+ = aPX + bPX(PX)^\top(PX) + cPX(PX)^\top(PX)(PX)^\top(PX)$$
$$= P(aX + bXX^\top X + cXX^\top XX^\top X),$$

where the second equality is because of Property I. Therefore, we obtain that

$$\texttt{NewtonSchulz}(PX) = P \cdot \texttt{NewtonSchulz}(X),$$

which finishes the proof of Property II and thus the unbiased property of GUM. $\square$

B.2   Proof of Theorem 1

We first state the notations in the following proof writing. For simplicity, we assume that the total iteration number $T = K\tau$. For $k = 0, \ldots, K - 1$ in a specific period $t = 0, \ldots, \tau - 1$, Algorithm 2 is mathematically equivalent to the following formulation:

$$\tilde{G}_{t,k} = \begin{cases} \frac{1}{1-q_t} P_t P_t^\top G_{t,k}, & \text{if } \xi_t = 0 \\ \frac{1}{q_t}(I - P_t P_t^\top) G_{t,k}, & \text{else} \end{cases}$$

$$\tilde{M}_{t,k} = \beta \tilde{M}_{t,k-1} + (1 - \beta)\tilde{G}_{t,k}$$

$$W_{tK+k+1} = W_{tK+k} - \eta \texttt{NewtonSchulz}(\tilde{M}_{t,k})$$

where $G_{t,k}$ is the stochastic gradient obtained at W_{tK+k} and $\xi_t \sim \text{Bernoulli}(q_t)$ is the indicator random variable such that $\xi_t = 1$ means using full-rank update in period t. We assume that the full-rank probability $q_t \equiv q$ and step size $\eta_t \equiv \eta$ are constants. The equivalence of Algorithm 2 and this formulation is shown by Lemma 1. At the beginning of each period, we initialize P_t from $G_{t,0}$ and set $\tilde{M}_{t,-1} = 0$. Also, we denote $\nabla f_{t,k} \triangleq \nabla f(W_{tK+k})$ and $\text{msign}(X) \triangleq UV^\top$ for $X = U\Sigma V^\top$ as the SVD of X. Under Assumption 4, we have $\texttt{NewtonSchulz}(X) = \text{msign}(X)$. Note that here in the theoretical proof, we consider the damping, i.e., the $1 - \beta$ term in the update of $\tilde{M}_{t,k}$. Since we initialize $\tilde{M}_{t,k} = 0$ in each period, this damping will not affect the algorithm because the Newton-Schulz iteration is irrelevant to the input scale.

To help simplify the convergence proof, we also denote the residual of the projector as $R_t \in \mathbb{R}^{m \times (m-r)}$, i.e., we take $U_t = [P_t \ R_t] \in \mathbb{R}^{m \times m}$, which satisfies that $P_t^\top R_t = 0$, $R_t^\top P_t = 0$. Note that since we consider only the case $m \leq n$ here, we have $U_t U_t^\top = P_t P_t^\top + R_t R_t^\top = I$. We further define

$$Q_t \triangleq \begin{cases} P_t, & \text{if } \xi_t = 0 \\ R_t, & \text{else} \end{cases} \tag{3}$$

and the following auxiliary sequence

$$M_{t,k} = \beta M_{t,k-1} + (1 - \beta)G_{t,k} \tag{4}$$

with $M_{t,-1} = 0$, which is the exponential moving average of the real gradient. With these definitions, we have

$$\text{msign}\left(\tilde{M}_{t,k}\right) = \text{msign}\left(Q_t Q_t^\top M_{t,k}\right) = Q_t \text{msign}\left(Q_t^\top M_{t,k}\right), \tag{5}$$

where the equation is based on the fact that $Q_t^\top Q_t = I$.

We first make use of the smoothness assumption to obtain a one-step analysis.

Lemma 3 (One-step descent). *Under Assumption 2 and 4 and setting $\eta_t \equiv \eta$, for $t = 0, \ldots, \tau - 1$ and $k = 0, \ldots, K - 1$, it holds that*

$$f(W_{tK+k+1}) \leq f(W_{tK+k}) - \eta \left\| Q_t^\top \nabla f_{t,k} \right\|_* + \frac{1}{2}\eta^2 L_{\text{op}} + 2\eta \left\| M_{t,k} - \nabla f_{t,k} \right\|_*, \tag{6}$$

where Q_t is defined as (3).

Proof. Based on Assumption 2, we have the descent property

$$\begin{aligned} f(W_{tK+k+1}) \leq &f(W_{tK+k}) + \langle \nabla f_{t,K}, W_{tK+k+1} - W_{tK+k} \rangle + \frac{L_{\text{op}}}{2} \left\| W_{tK+k+1} - W_{tK+k} \right\|_{\text{op}}^2 \\ = &f(W_{tK+k}) - \eta \left\langle \nabla f_{t,K}, \text{msign}\left(\tilde{M}_{t,k}\right) \right\rangle + \frac{L_{\text{op}}\eta^2}{2} \left\| \text{msign}\left(\tilde{M}_{t,k}\right) \right\|_{\text{op}}^2 \\ = &f(W_{tK+k}) - \eta \left\langle M_{t,K}, \text{msign}\left(\tilde{M}_{t,k}\right) \right\rangle + \frac{L_{\text{op}}\eta^2}{2} \\ &+ \eta \left\langle M_{t,K} - \nabla f_{t,k}, \text{msign}\left(\tilde{M}_{t,k}\right) \right\rangle \\ \leq &f(W_{tK+k}) - \eta \left\langle M_{t,K}, \text{msign}\left(\tilde{M}_{t,k}\right) \right\rangle + \frac{L_{\text{op}}\eta^2}{2} + \eta \left\| M_{t,K} - \nabla f_{t,k} \right\|_*, \end{aligned}$$

where the last inequality is based on the fact that $\|\cdot\|_*$ and $\|\cdot\|_{\mathrm{op}}$ are dual norms and $\left\|\mathrm{msign}\left(\tilde{M}_{t,k}\right)\right\|_{\mathrm{op}} = 1$. Then we further deal with the second term on the right hand side:

$$
\begin{aligned}
-\left\langle M_{t,K}, \mathrm{msign}\left(\tilde{M}_{t,k}\right)\right\rangle &\overset{(5)}{=} -\left\langle M_{t,K}, Q_t \mathrm{msign}\left(Q_t^\top M_{t,k}\right)\right\rangle \\
&= -\left\langle Q_t^\top M_{t,K}, \mathrm{msign}\left(Q_t^\top M_{t,k}\right)\right\rangle = -\left\|Q_t^\top M_{t,k}\right\|_* \\
&\leq -\left\|Q_t^\top \nabla f_{t,k}\right\|_* + \left\|Q_t^\top \left(M_{t,k} - \nabla f_{t,k}\right)\right\|_* \\
&\leq -\left\|Q_t^\top \nabla f_{t,k}\right\|_* + \left\|M_{t,k} - \nabla f_{t,k}\right\|_*,
\end{aligned}
$$

where the last inequality is based on that $Q_t Q_t^\top \preceq I$. Then combining the inequalities, we can finish the proof. $\qquad\square$

Based on Lemma 3, we could find that a key to proving the convergence is the $\|M_{t,k} - \nabla f_{t,k}\|_*$ term. Let us define the following auxiliary sequences:

$$
\epsilon_{t,k} \triangleq M_{t,k} - \nabla f_{t,k}, \quad S_{t,k} \triangleq \nabla f_{t,k-1} - \nabla f_{t,k}, \quad N_{t,k} \triangleq G_{t,k} - \nabla f_{t,k} \tag{7}
$$

and additionally set $\nabla f_{t,-1} \triangleq \nabla f_{t,0}$ for all $t = 0, \ldots, \tau - 1$. Then we consider decomposing the desired ϵ_t based on the properties of moving average sequences.

Lemma 4 (Decompose $\epsilon_{t,k}$). *For $t = 0, \ldots, \tau - 1$ and $k = 0, \ldots, K - 1$, it holds that*

$$
\epsilon_{t,k} = \sum_{i=1}^{k} \beta^{k-i+1} S_{t,i} + (1 - \beta) \sum_{i=0}^{k} \beta^{k-i} N_{t,i} - \beta^k \nabla f_{t,0}. \tag{8}
$$

Proof. From the definition of $M_{t,k}$ in (4), we know that

$$
M_{t,k} = \beta M_{t,k-1} + (1 - \beta) G_{t,k},
$$

which implies that

$$
\begin{aligned}
\epsilon_t &= \beta (M_{t,k-1} - \nabla f_{t,k-1}) + \beta(\nabla f_{t,k-1} - \nabla f_{t,k}) + (1 - \beta)(G_{t,k} - \nabla f_{t,k}) \\
&= \beta \epsilon_{t,k-1} + \beta S_{t,k} + (1 - \beta) N_{t,k}.
\end{aligned}
$$

Then by applying the equality recursively and noting that $\epsilon_{t,0} = (1 - \beta) G_{t,0} - \nabla f_{t,0} = (1 - \beta) N_{t,0} - \beta \nabla f_{t,0}$, we conclude the proof. $\qquad\square$

Then we produce the next lemma to state the variance contraction properties of momentum for Muon, which has been explored for Normalized SGD [Cutkosky and Mehta, 2020] and SignSGD [Sun et al., 2023], and also for Muon [Li and Hong, 2025], but with different assumptions.

Lemma 5 (Variance Contraction). *Under Assumption 3, for $t = 0, \ldots, \tau - 1$ and $k = 0, \ldots, K - 1$, it holds that*

$$
\mathbb{E}\left[\left\|(1 - \beta) \sum_{i=0}^{k} \beta^{k-i} N_{t,i}\right\|_*\right] \leq \|V\|_* \sqrt{(1 - \beta^{2k})(1 - \beta)}. \tag{9}
$$

Proof. Based on Lemma 8 in An et al. [2025], for an arbitrary symmetric positive definite matrix $H \in \mathbb{R}^{m \times m}$, it holds that

$$
\begin{aligned}
\mathbb{E}\left[\left\|\sum_{i=0}^{k} \beta^{k-i} N_{t,i}\right\|_*\right] &\leq \mathbb{E}\left[\sqrt{\|H\|_* \mathrm{tr}\left(\left(\sum_{i=0}^{k} \beta^{k-i} N_{t,i}\right)^\top H^{-1} \left(\sum_{i=0}^{k} \beta^{k-i} N_{t,i}\right)\right)}\right] \\
&= \mathbb{E}\left[\sqrt{\|H\|_* \mathrm{tr}\left(\left(\sum_{i=0}^{k} \beta^{k-i} N_{t,i}\right) \left(\sum_{i=0}^{k} \beta^{k-i} N_{t,i}\right)^\top H^{-1}\right)}\right]
\end{aligned}
$$

$$\leq \sqrt{\|H\|_* \, \mathbb{E}\left[\mathrm{tr}\left(\left(\sum_{i=0}^{k} \beta^{k-i} N_{t,i}\right)\left(\sum_{i=0}^{k} \beta^{k-i} N_{t,i}\right)^{\top} H^{-1}\right)\right]}$$

$$= \sqrt{\|H\|_* \, \mathbb{E}\left[\mathrm{tr}\left(\left(\sum_{i=0}^{k} \beta^{2(k-i)} N_{t,i} N_{t,i}^{\top}\right) H^{-1}\right)\right]},$$

where the last inequality is based on the fact that $\mathbb{E}[\sqrt{X}] \leq \sqrt{\mathbb{E}[X]}$ and the last equality is based on the assumption that $N_{t,i}$ and $N_{t,j}$ are independent for $i \neq j$, which implies $\mathbb{E}[\mathrm{tr}(N_{t,i} N_{t,j}^{\top} H)] = 0$. Then taking $H = (VV^{\top})^{1/2}$ leads to

$$\sqrt{\|H\|_* \, \mathbb{E}\left[\mathrm{tr}\left(\left(\sum_{i=0}^{k} \beta^{2(k-i)} N_{t,i} N_{t,i}^{\top}\right) H\right)\right]} = \sqrt{\|V\|_* \, \mathbb{E}\left[\mathrm{tr}\left(\sum_{i=0}^{k} \beta^{2(k-i)} N_{t,i} N_{t,i}^{\top}(VV^{\top})^{-\frac{1}{2}}\right)\right]}$$

$$\leq \sqrt{\|V\|_* \sum_{i=0}^{k} \beta^{2(k-i)} \mathrm{tr}\left(VV^{\top}(VV^{\top})^{-\frac{1}{2}}\right)}$$

$$\leq \|V\|_* \sqrt{\frac{1 - \beta^{2k}}{1 - \beta^2}},$$

where the first inequality is based on Assumption 3 and the second inequality is by algebra. Then, combining the inequalities and multiplying $1 - \beta$ gives the result. $\qquad \square$

Lemma 6 (Bound $\mathbb{E}\|\epsilon_{t,k}\|_*$). *Under Assumption 3, for $t = 0, \ldots, \tau - 1$ and $k = 0, \ldots, K - 1$, it holds that*

$$\mathbb{E}[\|\epsilon_{t,k}\|_*] \leq \frac{1 - \beta^k}{1 - \beta} L_{\mathrm{op}} \eta + \sqrt{(1 - \beta^{2k})(1 - \beta)} \|V\|_* + \beta^k \mathbb{E}\left[\|\nabla f_{t,0}\|_*\right]. \tag{10}$$

Proof. Based on Lemma 4, it holds that

$$\mathbb{E}\left[\|\epsilon_{t,k}\|_*\right] = \mathbb{E}\left[\left\|\sum_{i=1}^{k} \beta^{k-i+1} S_{t,i} + (1 - \beta)\sum_{i=0}^{k} \beta^{k-i} N_{t,i} - \beta^k \nabla f_{t,0}\right\|_*\right]$$

$$\leq \sum_{i=1}^{k} \beta^{k-i+1} \|S_{t,i}\|_* + \left\|(1 - \beta)\sum_{i=0}^{k} \beta^{k-i} N_{t,i}\right\|_* + \left\|\beta^k \nabla f_{t,0}\right\|_*,$$

where the inequality is based on the triangular inequality. For the first term in the RHS, it holds that

$$\|S_{t,i}\|_* = \|\nabla f_{t,i-1} - \nabla f_{t,i}\|_* \leq L_{\mathrm{op}} \|W_{tK+i-1} - W_{tK+i}\| = L_{\mathrm{op}} \eta.$$

Thus we have

$$\mathbb{E}\left[\|\epsilon_{t,k}\|_*\right] \leq \sum_{i=1}^{k} \beta^{k-i+1} L_{\mathrm{op}} \eta + \mathbb{E}\left[\left\|(1 - \beta)\sum_{i=0}^{k} \beta^{k-i} N_{t,i}\right\|_*\right] + \mathbb{E}\left[\|\beta^k \nabla f_{t,0}\|_*\right]$$

$$\overset{(9)}{\leq} \sum_{i=1}^{k} \beta^{k-i+1} L_{\mathrm{op}} \eta + \sqrt{(1 - \beta^{2k})(1 - \beta)} \|V\|_* + \beta^k \mathbb{E}\left[\|\nabla f_{t,0}\|_*\right]$$

$$\leq \frac{1 - \beta^k}{1 - \beta} L_{\mathrm{op}} \eta + \sqrt{(1 - \beta^{2k})(1 - \beta)} \|V\|_* + \beta^k \mathbb{E}\left[\|\nabla f_{t,0}\|_*\right],$$

which concludes the proof. $\qquad \square$

We need to further determine the expected projected gradient for $\nabla f_{t,0}$.

Lemma 7 (Expected projected gradient). *For $t = 0, \ldots, \tau - 1$, it holds that*

$$\mathbb{E}\left[\|Q_t^{\top} \nabla f_{t,0}\|_*\right] \geq \min\{q, 1 - q\} \mathbb{E}\left[\|\nabla f_{t,0}\|_*\right]. \tag{11}$$

Proof. Based on the algorithm, we know that ξ_t and W_{tK} are independent, which means that

$$\mathbb{E}\left[\left\|Q_t^\top \nabla f_{t,0}\right\|_*\right] = (1-q)\mathbb{E}\left[\left\|P_t^\top \nabla f_{t,0}\right\|_*\right] + q\mathbb{E}\left[\left\|R_t^\top \nabla f_{t,0}\right\|_*\right].$$

Because we have $U_t = [P_t\ R_t]$ that satisfies $U_t^\top U_t = U_t U_t^\top = I$, it holds for any $X \in \mathbb{R}^{m \times n}$ that

$$
\begin{aligned}
\left\|P_t^\top X\right\|_* + \left\|R_t^\top X\right\|_* &= \mathrm{tr}\left(\left(X^\top P_t P_t^\top X\right)^{\frac{1}{2}}\right) + \mathrm{tr}\left(\left(X^\top R_t R_t^\top X\right)^{\frac{1}{2}}\right) \\
&\geq \mathrm{tr}\left(\left(X^\top (P_t P_t^\top + R_t R_t^\top)X\right)^{\frac{1}{2}}\right) \\
&= \mathrm{tr}\left(\left(X^\top X\right)^{\frac{1}{2}}\right) = \|X\|_*.
\end{aligned}
$$

Therefore, we have

$$
\begin{aligned}
\mathbb{E}\left[\left\|Q_t^\top \nabla f_{t,0}\right\|_*\right] &= (1-q)\mathbb{E}\left[\left\|P_t^\top \nabla f_{t,0}\right\|_*\right] + q\mathbb{E}\left[\left\|R_t^\top \nabla f_{t,0}\right\|_*\right] \\
&\geq \min\{q, 1-q\}\left(\mathbb{E}\left[\left\|P_t^\top \nabla f_{t,0}\right\|_*\right] + \mathbb{E}\left[\left\|R_t^\top \nabla f_{t,0}\right\|_*\right]\right) \\
&\geq \min\{q, 1-q\}\,\mathbb{E}\left[\left\|\nabla f_{t,0}\right\|_*\right],
\end{aligned}
$$

which completes the proof. $\qquad\square$

With the lemmas in hand, we are able to prove Theorem 1.

Proof of Theorem 1. Based on Lemma 3, for $t = 0, \ldots, \tau-1$ and $k = 0, \ldots, K-1$, it holds that

$$
\begin{aligned}
f(W_{tK+k+1}) &\overset{(6)}{\leq} f(W_{tK+k}) - \eta\left\|Q_t^\top \nabla f_{t,k}\right\|_* + \frac{1}{2}\eta^2 L_{\mathrm{op}} + 2\eta\left\|M_{t,k} - \nabla f_{t,k}\right\|_* \\
&= f(W_{tK+k}) - \eta\left\|Q_t^\top \nabla f_{t,k}\right\|_* + \frac{1}{2}\eta^2 L_{\mathrm{op}} + 2\eta\left\|\epsilon_{t,k}\right\|_*,
\end{aligned}
$$

where Q_t is defined in (3) and $\epsilon_{t,k}$ is defined in (7). Then, after rearrangement and summation over k and taking expectation, we have

$$
\begin{aligned}
\sum_{k=0}^{K-1} \eta\mathbb{E}\left[\left\|Q_t^\top \nabla f_{t,k}\right\|_*\right] &\leq \mathbb{E}\left[f(W_{tK}) - f(W_{(t+1)K})\right] + \frac{1}{2}\eta^2 K L_{\mathrm{op}} + 2\eta\sum_{k=0}^{K-1}\mathbb{E}\left[\left\|\epsilon_{t,k}\right\|_*\right] \\
&\overset{(10)}{\leq} \mathbb{E}\left[f(W_{tK}) - f(W_{(t+1)K})\right] + \frac{1}{2}\eta^2 K L_{\mathrm{op}} \\
&\quad + 2\eta\sum_{k=0}^{K-1}\left(\frac{1-\beta^k}{1-\beta}L_{\mathrm{op}}\eta + \left(\sqrt{(1-\beta^{2k})(1-\beta)} + \beta^k\right)\|V\|_*\right) \\
&\leq \mathbb{E}\left[f(W_{tK}) - f(W_{(t+1)K})\right] + \eta^2 K L_{\mathrm{op}}\left(\frac{1}{2} + \frac{2(1-\beta^K)}{1-\beta}\right) \\
&\quad + 2\eta\left(\sqrt{(1-\beta^{2k})(1-\beta)}\|V\|_* + \beta^k\mathbb{E}\left[\left\|\nabla f_{t,0}\right\|_*\right]\right).
\end{aligned}
$$

Since W_{tK+k} is dependent on Q_t, it would be difficult to bound $\mathbb{E}[\|Q_t \nabla f_{t,k}\|_*]$ for $k \geq 1$. We therefore consider

$$
\begin{aligned}
\sum_{k=0}^{K-1} \eta\mathbb{E}\left[\left\|Q_t^\top \nabla f_{t,k}\right\|_*\right] &\geq \sum_{k=0}^{K-1} \eta\mathbb{E}\left[\left\|Q_t^\top \nabla f_{t,0}\right\|_*\right] - \sum_{k=0}^{K-1} \eta\mathbb{E}\left[\left\|Q_t^\top (\nabla f_{t,k} - \nabla f_{t,0})\right\|_*\right] \\
&\geq \sum_{k=0}^{K-1} \eta\mathbb{E}\left[\left\|Q_t^\top \nabla f_{t,0}\right\|_*\right] - \sum_{k=1}^{K-1} \eta\mathbb{E}\left[\left\|\nabla f_{t,k} - \nabla f_{t,0}\right\|_*\right] \\
&\geq \sum_{k=0}^{K-1} \eta\mathbb{E}\left[\left\|Q_t^\top \nabla f_{t,0}\right\|_*\right] - \sum_{k=1}^{K-1} \eta\sum_{l=1}^{k}\mathbb{E}\left[\left\|\nabla f_{t,l} - \nabla f_{t,l-1}\right\|_*\right] \\
&\geq \sum_{k=0}^{K-1} \eta\mathbb{E}\left[\left\|Q_t^\top \nabla f_{t,0}\right\|_*\right] - \sum_{k=1}^{K-1} \eta L_{\mathrm{op}}\sum_{l=1}^{k}\mathbb{E}\left[\left\|W_{tK+l} - W_{tK+l-1}\right\|_{\mathrm{op}}\right]
\end{aligned}
$$

22

$$\geq K\eta\mathbb{E}\left[\left\|Q_t^\top\nabla f_{t,0}\right\|_*\right] - \frac{K^2}{2}\eta^2 L_{\mathrm{op}},$$

where the first and third inequalities are based on the triangular inequality and the second inequality is based on that $Q_t Q_t^\top \preceq I$. The second last inequality uses Assumption 2. Then we combine the above inequalities and further sum up over t and use Assumption 1 to obtain that

$$\sum_{t=0}^{\tau-1} K\mathbb{E}\left[\left\|Q_t^\top\nabla f_{t,0}\right\|_*\right] \leq \frac{f(W_0) - f^*}{\eta} + \eta K\tau L_{\mathrm{op}}\left(\frac{K+1}{2} + \frac{2(1-\beta^K)}{1-\beta}\right)$$

$$+ 2\tau K\sqrt{(1-\beta^{2K})(1-\beta)}\left\|V\right\|_* + \sum_{t=0}^{\tau-1}\frac{2(1-\beta^K)}{1-\beta}\mathbb{E}\left[\left\|\nabla f_{t,0}\right\|_*\right].$$

Combining Lemma 7, we have

$$K\mathbb{E}\left[\left\|Q_t^\top\nabla f_{t,0}\right\|_*\right] - \frac{2(1-\beta^K)}{1-\beta}\mathbb{E}\left[\left\|\nabla f_{t,0}\right\|_*\right] \geq \frac{K\alpha}{2}\mathbb{E}\left[\left\|\nabla f_{t,0}\right\|_*\right]$$

where $\alpha \triangleq \min\{q, 1-q\}$ and we take $\alpha > \frac{2}{K}$ and $1 - \beta \geq \frac{2}{K\alpha}$. Thus, we can obtain that

$$\frac{\alpha}{2\tau}\sum_{t=0}^{\tau-1}\mathbb{E}\left[\left\|\nabla f_{t,0}\right\|_*\right] \leq \frac{f(W_0) - f^*}{\eta T} + \eta L_{\mathrm{op}}\left(\frac{K+1}{2} + \frac{2}{1-\beta}\right) + 2\sqrt{1-\beta}\left\|V\right\|_*$$

$$\leq \frac{f(W_0) - f^*}{\eta T} + \eta L_{\mathrm{op}}\left(\frac{K+1}{2} + K\alpha\right) + 2\sqrt{1-\beta}\left\|V\right\|_*$$

By choosing the hyperparameter as

$$\eta = \sqrt{\frac{TL_{\mathrm{op}}\left(\frac{K+1}{2} + K\alpha\right)}{f(W_0) - f^*}}, \quad \beta = 1 - \frac{2}{K\alpha}, \quad K = \max\left\{1, \min\left\{\frac{\sigma\sqrt{T}}{\sqrt{\alpha L(f(W_0) - f^*)}}, T\right\}\right\}, \quad (12)$$

we can obtain that

$$\min_{t=0,\ldots,\frac{T}{K}-1}\mathbb{E}\left[\left\|\nabla f(W_{tK})\right\|\right] \leq \mathcal{O}\left(\frac{1}{\alpha}\sqrt{\frac{L_{\mathrm{op}}\Delta}{T}} + \left(\frac{L_{\mathrm{op}}\Delta\left\|V\right\|_*^2}{\alpha^5 T}\right)^{\frac{1}{4}} + \frac{\left\|V\right\|_*}{\sqrt{\alpha^3 T}}\right),$$

with $\Delta \triangleq f(W_0) - f^*$, which finishes the proof. $\qquad\square$

C Training Setup and Hyperparameters

C.1 Fine-tuning Setup

In our experiments, we slightly modify the full-rank update rule (2) for GUM by multiplying $(1 - q_{t,\ell})$ on $-P_{t,\ell}P_{t,\ell}^\top G_{t,k,\ell}$. This modification still preserves the unbiased property while being able to recover the original full-parameter Muon algorithm by setting $q_{t,\ell} = 1$.

We utilize LMFlow [Diao et al., 2023][*] to perform full-parameter fine-tuning, GaLore tuning, and GUM tuning. We set the number of training epochs for all fine-tuning scenarios to 1. All experiments were conducted on a single NVIDIA H100 GPU with 80 GB of memory.

We explored a range of learning rates from 8×10^{-6} to 1×10^{-4}, applying this range to Full Parameter Training, GaLore, and GUM. For GaLore, we fixed the rank $r = 512$ and applied it uniformly across all layers. In the case of GUM, the number of layers (γ) selected for full-rank updates was set to 2 for all models. The sampling interval K, which defines the number of update steps between each layer selection, was varied between 10 and 300, depending on factors such as dataset size, batch size, and total training steps. The models covered in this paper can be found in Table 5.

---

[*]https://github.com/OptimalScale/LMFlow

Table 5: Baseline Model Configurations

Model Name	# Params	# Layers	Model Dim
LLaMA-3-8B	8 B	32	4096
Qwen-2.5-7B	7 B	28	3584
Gemma-2-9B	9 B	42	3584

C.2 Fine-tuning Hyperparameters

We began our study by conducting a grid search over two key hyperparameters: (i) the learning rate and (ii) the number of sampling layers used for full-rank updates. Given the strong empirical performance of the GaLore method, we fixed the rank to $r = 512$. The learning rate was explored within the range $\{8 \times 10^{-6}, 2 \times 10^{-5}, 4 \times 10^{-5}, 6 \times 10^{-5}, 8 \times 10^{-5}, 1 \times 10^{-4}\}$, applied consistently across full parameter training, GaLore, and GUM. For GaLore, we followed the official `Transformers` implementation [*], using the default settings and aligning the learning rate with the full parameter training. With respect to the number of sampling layers, and in accordance with Table 3, we selected values that did not exceed the GPU memory cost of GaLore. As a result, $\gamma = 2$ was used in most GUM configurations. The sampling period K was uniformly set to 200 for all models. A detailed summary of the optimal hyperparameter values identified for each setting is provided in Table 6.

Table 6: Optimal settings for each method were determined through hyperparameter search: FT (Full-parameter Training)-AdamW, FT-Muon, GaLore, and GUM.

Model	FT-AdamW	FT-Muon	GaLore		GUM		
	lr	lr	lr	Rank	lr	γ	K
LLaMA-3-8B	3×10^{-5}	7×10^{-5}	9×10^{-5}	512	1×10^{-4}	2	200
Qwen-2.5-7B	1×10^{-5}	5×10^{-5}	7×10^{-5}	512	7×10^{-5}	2	200
Gemma-2-9B	–	4×10^{-5}	4×10^{-5}	512	6×10^{-5}	2	200

C.3 Pre-training Hyperparameters

In our experiments, we utilize C-optim [*] for the pre-training. Following standard protocol, we fixed the LLaMA context length to 1024 tokens. Similar to the fine-tuning setup, we made a grid search on learning rate and the number of sampling layers. The sampling period K was set to 100 for 130M and 350M models, 50 for the 60M model. A detailed summary of the optimal hyperparameter values identified for each setting is provided in Table 7.

Table 7: Optimal settings for each method were determined through hyperparameter search: AdamW, Muon, Fira, GaLore, and GUM.

Model	AdamW	Muon	Fira		GaLore		GUM		
	lr	lr	lr	Rank	lr	Rank	lr	γ	K
LLaMA-60M	3×10^{-3}	1×10^{-2}	9×10^{-3}	256	9×10^{-3}	256	9×10^{-3}	4	50
LLaMA-130M	2×10^{-3}	5×10^{-3}	5×10^{-3}	256	5×10^{-3}	256	5×10^{-3}	4	100
LLaMA-350M	1×10^{-3}	3×10^{-3}	3×10^{-3}	256	3×10^{-3}	256	3×10^{-3}	6	100

---

[*]https://github.com/jiaweizzhao/GaLore
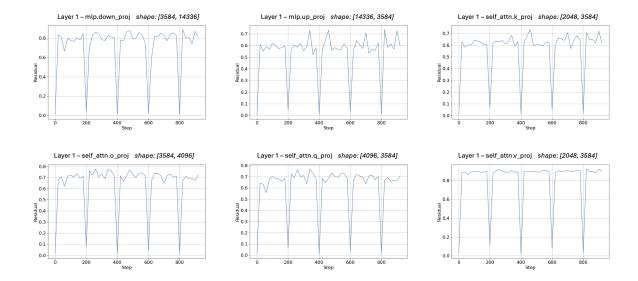[*]https://github.com/kyleliang919/C-Optim

Figure 4: Residual ($\chi_t = \|G_t^u - G_t^p\|_{\mathrm{F}}/\|G_t^u\|_{\mathrm{F}}$) between GaLore's projected and original gradients across different blocks during **Gemma-2-9B** fine-tuning. High residuals persist throughout training (except for the iterations with projector updates), revealing systematic bias in GaLore updates.

D Additional Experimental Results

D.1 Bias in GaLore

To further illustrate how significant the bias in low-rank projection methods is, we analyze the residuals between low-rank projected gradients and the original full-rank gradients across multiple layers during the fine-tuning of the **Gemma-2-9B** model on the **GPT-4-LLM** dataset. The residual is computed as follows:

$$\chi_t = \frac{\|G_t^u - G_t^p\|_{\mathrm{F}}}{\|G_t^u\|_{\mathrm{F}}}, \tag{13}$$

where G_t^u represents the original gradient at iteration t without projection, and G_t^p denotes the low-rank projected gradients in GaLore-Muon. We can see that χ_t presents the relative error between the original gradients and the projected gradients at iteration t, showing how much the projection operation makes the gradient estimation biased from the original one. We measure this relative error for each block of parameters along the trajectory of the GaLore-Muon algorithm every 20 iterations. The projector update frequency is set to 200, and the projection rank is 512. We use a batch size of 16 and a learning rate of 7×10^{-5}. For demonstration purposes, we specifically select the self-attention and MLP weights at layer 10.

As depicted in Figure 4, the relative error shows a periodic curve. It is relatively small (around $0 - 20\%$) in the iteration t such that t is a multiple of the update frequency 200, where the projector is updated based on the gradient. Since the GaLore projector is chosen as the singular vectors of the largest singular values of the current gradient, it is a good low-rank projector for the current gradient, which results in this small error. [*] However, we can see that the relative error rapidly increases after this and achieves even higher than $60 - 80\%$ in less than 20 iterations. This implies that although the low-rank projection of GaLore doesn't hurt much in the first iteration, it makes little sense for the following gradients, since the projection produces a really high relative error. Such a high relative error demonstrates a remarkably significant bias between the low-rank projected gradients and the original gradients, and between GaLore and the original gradient algorithm, highlighting the need to derive an unbiased low-rank projection algorithm.

---

[*]Note that while the projector is good for the stochastic gradient used in the algorithm, it can still be a large obstacle to the convergence, as shown in Figure 1.
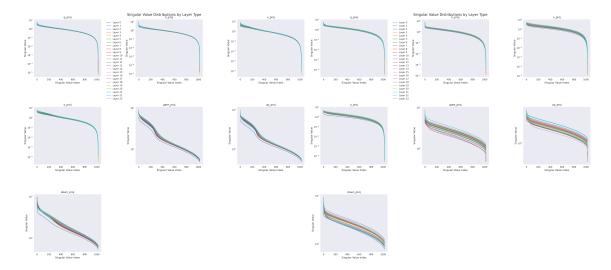
Figure 5: **Detailed Singular Value Distribution. Left**: GaLore. **Right**: GUM. It can be observed that GaLore has a sudden magnitude drop in the tail distribution of singular values in `gate proj` and `up proj` modules. GUM generally demonstrates smoother and more long-tailed singular value distributions. Furthermore, GUM has a differentiated spectrum across different layers, while this phenomenon is much weaker in GaLore.

D.2 Singular Value Distribution of Model Weights

As shown in Figure 5, GUM demonstrates a smoother and more long-tailed singular value distribution than GaLore, especially in modules of `gate proj` and `up proj`. The spectrums are also more differentiated and have a non-trivial diversity across layers in GUM.

E Broader Impacts

Memory-efficient training techniques are critical for scalable LLM development and for democratizing customized LLMs for broader societal use. Improving theoretical guarantees provides insights for the invention of new methods with enhanced performance, leading to reduced computational resource consumption and lower carbon dioxide emissions.

F Limitations

The technique of sampled high-rank updates inherently introduces high variance into the per-iteration updates when the sampling probability is low, which leads to instability in the training procedure and requires more careful tuning of the hyperparameters. To alleviate this issue, standard theoretical tools for variance reduction can be employed [Johnson and Zhang, 2013, Needell et al., 2014, Ge et al., 2019a], which we leave for future work here. The analysis can also be combined with other acceleration [Zhang and Xiao, 2017, Ge et al., 2019b, Pan et al., 2021, 2023, Defazio et al., 2024, Liu et al., 2025b] and generalization techniques [Arjovsky et al., 2019, Foret et al., 2020, Hao et al., 2025], whose properties are worth investigating as open problems. The algorithm's empirical performance and computational cost in other types of models [Devlin et al., 2019, Rombach et al., 2022, Pan et al., 2022, Liu et al., 2023, Gu and Dao, 2023, Hu et al., 2024, Wang et al., 2025, Mu and Lin, 2025] and applications [Xia et al., 2023, Peebles and Xie, 2023, Pan et al., 2025] also remain as interesting questions.

G The Use of Large Language Models

ChatGPT and GPT-5 were adopted to polish the writing of the paper, where all revised sentences were double-checked by the authors. OpenAI Deep Research was utilized for finding dataset licenses.

H   Licenses

For mathematical reasoning tasks in LLM fine-tuning, the training dataset comes from 4 different sources: DART-Math [Tong et al., 2024], UltraInteract [Yuan et al., 2024], MathInstruct [Yue et al., 2023], and Orca-Math [Mitra et al., 2024], with their licenses listed in Table 8. Other datasets and benchmarks are also available in the same table.

For code repositories, LMFlow [Diao et al., 2023] is released under Apache-2.0 license.

Training Datasets	#Samples	Kind	License
teknium/GPT4-LLM-Cleaned[*]	55K	Instruction	CC BY-NC 4.0
DART-Math[*] [Tong et al., 2024]	591K	Math	MIT
openbmb/UltraInteract_sft[*] [Yuan et al., 2024]	289K	Reasoning	MIT
TIGER-Lab/MathInstruct[*] [Yue et al., 2023]	262K	Reasoning	MIT
microsoft/orca-math-word-problems-200k[*] [Mitra et al., 2024]	200K	Math	MIT
C4 corpus[*] [Raffel et al., 2023]	>1B	Commonsense	ODC-BY
IFEval [Zhou et al., 2023]	0.5K	Instruction	Apache-2.0
GSM8K [Cobbe et al., 2021b]	7.5K	Math	MIT
ARC-E [Clark et al., 2018]	5.2K	Instruction	CC-BY-SA-4.0
ARC-C [Clark et al., 2018]	2.6K	Instruction	CC-BY-SA-4.0
HellaSwag [Zellers et al., 2019b]	10K	Commonsense reasoning	MIT
PIQA[*] [Bisk et al., 2020]	3K	Commonsense reasoning	Academic Free License v. 3.0
SIQA [Sap et al., 2019]	2.2K	Commonsense reasoning	CC-BY-4.0 [Li et al., 2024]
Winogrande[*] [Sakaguchi et al., 2021b]	1.8K	Commonsense reasoning	CC-BY
OBQA [Mihaylov et al., 2018b]	5.9K	Commonsense reasoning	(permissive open license)[*]

Table 8: Licenses of training datasets and benchmarks. Here, the number of samples for benchmarks only counts the test set.

---

[*] https://huggingface.co/datasets/teknium/GPT4-LLM-Cleaned
[*] https://huggingface.co/datasets/hkust-nlp/dart-math-uniform
[*] https://huggingface.co/datasets/openbmb/UltraInteract_sft
[*] https://huggingface.co/datasets/TIGER-Lab/MathInstruct
[*] https://huggingface.co/datasets/microsoft/orca-math-word-problems-200k
[*] https://huggingface.co/datasets/allenai/c4
[*] https://github.com/ybisk/ybisk.github.io/tree/master/piqa
[*] https://github.com/allenai/winogrande
[*] The OpenBookQA dataset is released under a permissive open license, making it freely available for academic research. In practice, sources indicate that the dataset is in the public domain or under a very permissive license. For example, a Kaggle distribution of OpenBookQA explicitly labels it CC0 1.0 Universal (Public Domain) (https://www.kaggle.com/datasets/thedevastator/openbookqa-a-new-dataset-for-advanced-question-a). Similarly, a curated dataset list reports OpenBookQA's license as Apache 2.0 (https://github.com/lmmlzn/Awesome-LLMs-Datasets). Both of these licenses allow unrestricted use, redistribution, and modification of the data, including for academic purposes.